ISTANBUL TECHNICAL UNIVERSITY ★ GRADUATE SCHOOL

STATIC MODELLING OF AN OPEN-CYCLE LIQUID-PROPELLANT ROCKET ENGINE

M.Sc. THESIS

Turan ÇOPUROĞLU

Department of Aeronautical and Astronautical Engineering

Aeronautical and Astronautical Engineering Programme

JANUARY 2026

ISTANBUL TECHNICAL UNIVERSITY ★ GRADUATE SCHOOL

STATIC MODELLING OF AN OPEN-CYCLE LIQUID-PROPELLANT ROCKET ENGINE

M.Sc. THESIS

Turan ÇOPUROĞLU
(511221140)

Department of Aeronautical and Astronautical Engineering

Aeronautical and Astronautical Engineering Programme

Thesis Advisor: Prof. Dr. Fırat Oğuz EDİS

JANUARY 2026

ISTANBUL TEKNİK ÜNİVERSİTESİ ★ LİSANSÜSTÜ EĞİTİM ENSTİTÜSÜ

AÇIK ÇEVRİM SIVI YAKITLI ROKET MOTORUNUN STATİK MODELLENMESİ

YÜKSEK LİSANS TEZİ

Turan ÇOPUROĞLU
(511221140)

Uçak ve Uzay Mühendisliği Anabilim Dalı

Uçak ve Uzay Mühendisliği Programı

Tez Danışmanı: Prof. Dr. Fırat Oğuz EDİS

OCAK 2026

Turan ÇOPUROĞLU, a M.Sc. student of İTU Graduate School student ID 511221140 successfully defended the thesis/dissertation entitled "STATIC MODELLING OF AN OPEN-CYCLE LIQUID-PROPELLANT ROCKET ENGINE", which he prepared after fulfilling the requirements specified in the associated legislations, before the jury whose signatures are below.

Thesis Advisor : **Prof. Dr. Fırat Oğuz EDİS** ....
Istanbul Technical University

Jury Members : **Prof. Dr. Aydın MISIRLIOĞLU** ....
Istanbul Technical University

Assistant Professor Serhat YILMAZ ....
National Defence University

Date of Submission : 27.12.2025
Date of Defense : 29.01.2026

To my family,

FOREWORD

This thesis was written with the harmony of industry experience and academic background. The subject of this study is the modelling of a liquid-propellant rocket engine and the comprehensive analysis of its results. The motivation of this study comes from ROKETSAN, where I have proudly worked since 2021.

I would like to express my deepest gratitude to my thesis advisor, Prof. Dr. Fırat Oğuz EDİS, for his invaluable guidance, insightful feedback, and continuous support throughout the course of this research. His academic guidance has played a crucial role in shaping the direction of this research, enhancing the robustness of its methodology, and notably increasing the quality and significance of the outcomes.

I am also grateful to my family for their unconditional support and encouragement throughout my master's program.

January 2026 Turan ÇOPUROĞLU

TABLE OF CONTENTS

ABBREVIATIONS

0D	: Zero Dimension
1D	: One Dimension
CEA	: Chemical Equilibrium with Applications
DLR	: Deutsches Zentrum für Luft- und Raumfahrt e.V.
ESA	: European Space Agency
FCV	: Fuel Control Valve
GG	: Gas Generator
GEO	: Geo-Synchronous Earth Orbit
GFSSP	: Generalized Fluid System Simulation Program
LEO	: Low Earth Orbit
LH_2	: Liquid Hydrogen
LN	: Liquid Nitrogen
LOX	: Liquid Oxygen
LPR2	: Liquid Rocket Propulsion 2
LPRE	: Liquid-Propellant Rocket Engine
KARI	: Korean Aerospace Research Institute
KSLV	: Korean Space Launch Vehicle
LVM3	: Launch Vehicle Mark-3
NASA	: National Aeronautics and Space Administration
NIST	: National Institute of Standards and Technology
MFR	: Mass Flow Rate
ISRO	: Indian Space Research Organization
O/F	: Oxidizer-to-Fuel Ratio
OCV	: Oxidizer Control Valve
P&ID	: Piping and Instrumentation Diagram
ROCETS	: Rocket Engine Transient Simulation
RP-1	: Rocket Propellant – 1
RPA	: Rocket Propulsion Analysis

SC : Stage Combustion Cycle

SL : Sea Level

SSME : Space Shuttle Main Engine

SSO : Sun-Synchronous Earth Orbit

TC : Thrust Chamber

T/W : Thrust-to-Weight Ratio

SYMBOLS

ε	:	Expansion Ratio
γ	:	Specific Heat Ratio
a	:	Acceleration
M	:	Mach Number
ζ	:	Minimum Singular Pressure Drop Factor
R	:	Gas Constant per Unit Weight
r	:	Mixture Ratio
R	:	Rate Of the Global Reactions
PR	:	Pressure Ratio
Kv	:	Maximum Flow Capacity Coefficient
h	:	Specific Enthalpy
Cv	:	Maximum Flow Capacity Coefficient
Cq	:	Maximum Flow Coefficient
v_{exit}	:	Exit Velocity
v_2	:	Exhaust Velocity
m_o	:	Oxidizer mass flowrate
m_f	:	Fuel mass flowrate
$\dot{m}$	:	Mass Flowrate
g_0	:	Standard sea-level Gravitational Acceleration
T_c	:	Chamber Temperature
P_{exit}	:	Exit Pressure
$P_{environment}$	:	Environment Pressure
P_c	:	Chamber Pressure
$P_{ambient}$	:	Ambient Pressure
I_{sp}	:	Specific Impulse
A_{throat}	:	Throat Area
A_{nozzle}	:	Nozzle Area

P_{atm}	:	Atmospheric pressure
P	:	Static Pressure fluid
ρ	:	Density of fluid
V	:	Velocity of fluid
g	:	Gravitational Acceleration
h	:	Elevation

LIST OF TABLES

Page

LIST OF FIGURES

Page

STATIC MODELLING OF AN OPEN-CYCLE LIQUID-PROPELLANT ROCKET ENGINE

SUMMARY

Ensuring that a rocket engine meets the mission performance requirements is critical for the successful operation of launch vehicles. Compliance with these requirements is verified through qualification tests. To reduce test costs and enable faster decision-making during development, establishing a high-accuracy engine model is a priority. Throughout the engine development process, subsystem performance may deviate from expected values. The cumulative impact of these deviations can drive overall engine performance outside the specified requirements. Therefore, maintaining traceability through modelling during the development phase and making corrective decisions based on model outputs are essential.

In this thesis, an open-cycle liquid-propellant rocket engine is modeled. The model solves 16 nonlinear equations simultaneously to obtain 16 key performance variables that define the engine cycle. Once these key variables are determined, all remaining system performance outputs such as thrust, specific impulse, gas-generator temperature, and hydraulic pressure losses can be calculated. Using literature data, the model is applied to the KRE-075 engine and validated at the nominal design point. The largest discrepancy is observed in the gas-generator results and the turbine pressure ratio, reaching approximately 5 - 8%. This difference is attributed to the use of tabulated gas-property data from Huzel's book for the gas-generator solution under fuel-rich operating conditions.

Under off-design operating conditions, variations in the positions of the control valves located in the gas-generator lines and in the thrust-chamber fuel line are investigated. For engine throttling, the most dominant effect is found to be driven by the gas-generator oxidizer control valve position, followed by the gas-generator fuel control valve position. Changes in the thrust-chamber fuel control valve position have a limited influence on the overall engine behavior. However, this valve is beneficial to trim the thrust chamber mixture ratio (O/F).

The developed model produces solutions significantly faster than one-dimensional (1D) transient solvers and provides a detailed representation of the engine performance response to configuration changes. The model provides a practical, flexible and robust analysis for engine preliminary design stages. In this respect, the model is capable of supporting industrial engine development activities and can provide a common framework for both academic investigations and industrial design studies.

AÇIK ÇEVRİM SIVI YAKITLI ROKET MOTORUNUN STATİK MODELLENMESİ

ÖZET

Fırlatma araçlarında roket motorunun, belirlenen görev gereksinimlerini karşılayacak performansı sağlaması kritik öneme sahiptir. Bu uygunluk, motor performansının gereksinimler dâhilinde olduğunu gösteren kalifikasyon ve kabul testleri ile doğrulanır. Motor geliştirme test sayılarını azaltmak ve geliştirme sürecinde yer alan iteratif tasarım döngülerine yönelik daha hızlı tasarım kararları alabilmek fırlatma aracı geliştirme proje maliyeti açısından oldukça önemlidir. Dolayısıyla, fırlatma aracı geliştirme süreçleri içerisinde yüksek doğrulukta bir motor modelinin oluşturulması elzemdir.

Roket motoru geliştirme çalışmaları boyunca motoru oluşturan alt sistem performanslarında belirlenen ve hedeflenen performans çıktılarında sapmalar oluşabilir. Ürüne dönüşen bileşen, ünite ve alt komplelerde oluşabilecek performans sapmalarının birikimsel etkisi roket motorunun performansını tasarım gereksinimlerinin dışına çıkmasına neden olabilir. Bu riskin minimize edilebilmesi ve roket motor performansının hedeflenen gereksinimleri sağlayacak şekilde kalibre edilmesi gereklidir. Bu nedenle, geliştirme dönemi boyunca izlenebilirliğin modelleme ile sağlanması ve performans sapmalarına karşın sistem özelinde alınacak kararların model çıktıları üzerinden verilmesi önem taşır.

Bu tez kapsamında, açık çevrimli sıvı yakıtlı bir roket motoru olan gaz jeneratör çevrimli sıvı yakıtlı roket motorunun statik olarak modellenmesi gerçekleştirilmiştir. Geliştirilen statik model zamana bağlı bir çözüm içermemekte olup geçici rejim için modelleme yapmadığından statik model olarak adlandırılmıştır. Motorun bulunduğu çalışma rejiminde sağladığı kararlı hal performansını çıktı olarak türetmektedir. Çözüm içerisinde motoru oluşturan bileşen, ünite veya alt komplelere ait performans karakteristikleri girdi olarak kullanılmaktadır. İtki odası için alan oranı, enjektörler için boşaltma katsayıları, vanalar için akış katsayıları, pompalar için basma – akış eğrileri, türbin için verim eğrilerini, hidrolik hatlar için kayıp katsayıları girdi olarak kullanmaktadır.

Statik model, gaz jeneratör çevrimli sıvı yakıtlı roket motoru çevrimini tanımlayan 16 doğrusal olmayan denklemin nümerik olarak çözülmesine dayanmaktadır. Bu denklemler içerisinde yer alan 16 motor performans parametresi çözüm kökü olarak belirlenmektedir. Her iterasyonda güncellenen bu parametrelerin yakınsaması ve denklemlere ait artık değerlerinin sıfıra yaklaşması ile birlikte çözüm tamamlanmaktadır.

Statik modelde kullanılan denklemlerin çözülmesi sonucunda elde edilen 16 kritik performans parametresi; turbopompa devri, pompa verimleri, itki odası ve gaz jeneratörüne giden oksitleyici ve yanıcı debileri, yanma odası basınçları, türbin

verimi, türbin adyabatik hızı, türbin çıkışındaki gaz sıcaklığı, türbin çıkışındaki gaz basıncı, ve türbinde yer alan lüle çıkışındaki Mach sayısını kapsamaktadır. Bu ana değişkenler belirlendikten sonra motor itkisi, vakum özgül itkisi gibi elde edilmek istenen diğer tüm sistem performans çıktıları hesaplanabilmektedir.

Model çözümünde yer alan itki odasındaki yanma odası basıncını hesaplarken ihtiyaç duyulan yanma ürünü gaz özelliklerinin (örneğin, sıcaklık, özgül ısı oranı ve gaz sabiti) elde edilmesi amacıyla CEA, "Chemical Equilibrium and Applications", kullanılmaktadır. Tez kapsamında çalışılan roket motorunda gaz jeneratörü yanıcı zengin çalışmaktadır. Yanıcı zengin yanma reaksiyonları için CEA kullanımı uygun olmadığından dolayı gaz jeneratöründe yer alan yanma odası basınç hesaplamalarında kullanılan gaz özellikleri uygun korelasyonlar kullanılarak elde edilmiştir. Kullanılan korelasyonlar ile deneysel sonuçlar arasındaki farklar tezde detaylı olarak verilmiştir.

Statik model kullanılarak Kore Havacılık ve Uzay Araştırma Enstitüsü tarafından geliştirilen KRE-075 gaz jeneratör çevrimli sıvı yakıtlı roket motoru için performans sonuçları elde edilmiştir. Modelde kullanılan ve motoru oluşturan bileşen, ünite ve alt sistemlere ait girdi verileri KRE-075'in geliştirme sürecinde gerçekleştirilmiş olan ve açık literatürde yer alan testler ile analizlerden temin edilmiştir.

Model doğrulaması amacıyla statik model sonuçları KRE-075 motoruna ait açık literatürde yer alan performans verileri ile karşılaştırılmıştır. Karşılaştırma sonucunda, tasarım verileri ile model çıktıları arasındaki farkın gaz jeneratörü toplam debisi ve yanma odası basıncı için yaklaşık %5, türbin basınç oranı için ise yaklaşık %8 olduğu belirlenmiştir. Gaz jeneratörü yanma odası basıncı hesaplanmasında yer alan gaz özelliklerinin belirlenmesi amacıyla kullanılan korelasyonlardan kaynaklanan bu sapmalar makul ve kabul edilebilir seviyede değerlendirilmiştir.

KRE-075 motorunda motor debilerinin kontrolünü sağlayan 3 adet kontrol vanası mevcuttur. Bunlardan ikisi gaz jeneratörü oksitleyici hattı ve yanıcı hattında yer almakta olup diğeri itki odası yanıcı hattında yer almaktadır. Tez kapsamında, motorun tasarım noktası dışındaki motor performans haritasının türetilebilmesi amacıyla, 3 kontrol vanasının farklı kısılma oranları için motordaki performans cevabı türetilmiştir. Böylelikle, motoru oluşturan bileşen, ünite ve alt sistemlerin birbirleriyle etkileşimi detaylandırılarak motor performansı üzerindeki etkileri gösterilmiştir.

Gaz jeneratörü oksitleyici hattında bulunan kontrol vanasının açıklığının arttırılması ile birlikte gaz jeneratöründeki yanma odası karışım oranının arttığı ve türbine beslenen gaz sıcaklığının yükseldiği belirlenmiştir. Artan gaz sıcaklığı türbin gücünü artırmakta, pompalara aktarılan gücün yükselmesi ise hem oksitleyici hem de yanıcı pompalar tarafından çekilen debilerin artmasına neden olmaktadır. Bu durum gaz jeneratörüne giden yanıcı debisinin de artışını sağlamaktadır. Gaz jeneratöründe üretilen gaz sıcaklığındaki artışa ek olarak, gaz jeneratörüne beslenen yanıcı debisinin yükselmesiyle türbine giren toplam kütlesel debinin kümülatif olarak artış göstermesi sonucunda, motorun itkisinin artırılması veya azaltılması işlemlerinde baskın kontrol değişkeninin gaz jeneratörü oksitleyici debisi olduğu görülmüştür.

Gaz jeneratörü yanıcı hattındaki kontrol vanasının açılması ise gaz jeneratöründeki karışım oranını azaltmakta ve türbine beslenen gaz sıcaklığının düşmesine neden olmaktadır. Sıcaklık düşüşüne bağlı olarak türbin gücü azalmakta, bu da pompalara aktarılan gücün ve pompaların çektiği debilerin düşmesine yol açmaktadır. Sonuç olarak gaz jeneratörüne beslenen oksitleyici debisi azalmaktadır. Bu nedenle, gaz jeneratörü oksitleyici kontrol vanasında gözlenen birikimsel etki burada ortaya çıkmamaktadır.

İtki odası yanıcı kontrol vanası pozisyon değişimlerinin sistem üzerindeki etkisinin sınırlı olduğu, buna karşın itki odası karışım oranının (O/F) dengelenmesi amacıyla uygun bir kontrol elemanı olduğu gösterilmiştir.

Geliştirilen model, bir boyutlu geçici rejim çözümlerine kıyasla çok daha hızlı çözüm üretmekte ve sistemdeki değişimlere verilen yanıtı ayrıntılı biçimde ortaya koymaktadır. Bu yönüyle model, endüstriyel motor geliştirme faaliyetlerine destek sağlayabilecek ve akademik çalışmalar için köprü niteliği taşıyabilecek bir araç olma niteliği taşımaktadır.

1. INTRODUCTION

1.1 Overview

In recent years, the development of launch vehicles has gained considerable momentum and has become a key area of competition in the fast-growing space sector. Growing global interest in access to space has led public and private organizations to invest in propulsion and orbital deployment technologies.

Under the "NewSpace" paradigm, missions have shifted toward smaller, lower-cost payloads, and more actors have entered the space industry. This change has brought a sharp increase in launch activity. In particular, launch attempts increased by about 70% between 2016 and 2021. Despite the increase in launch attempts, the success rate reached its lowest level in 2020. Figure 1.1 shows the number of launch attempts and the succes rate between 2006 and 2020. Cost and schedule limitations make sustainability a core design requirement, including minimizing orbital debris, post-mission disposal and reduced impacts on Earth's environment [1].

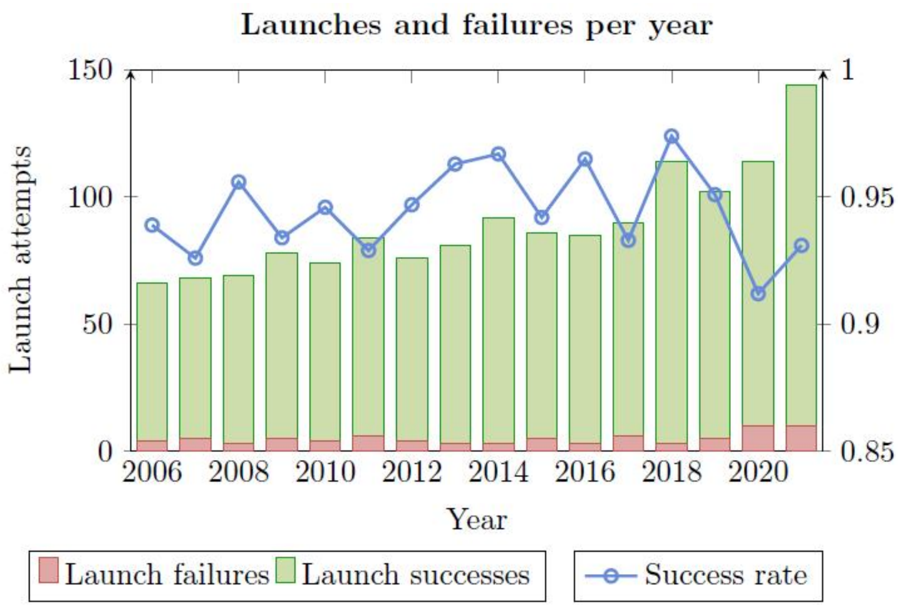

Figure 1.1: Launch Attempts and Success Rates Between 2006 – 2020 [1]

Fernandez et al. [1] classified launch-vehicle failure causes into eight subsystems: Propulsion (PROP), Trajectory and Attitude Control (TACS), Power Storage and Distribution (POW), Telemetry (TEL), Onboard Computer (OBC), Thermal Control (TCS), Structures (STR) and Separation (SEP). Figure 1.2 illustrates a key finding that propulsion accounts for 54% of failures. Among propulsion failures, only one involved a solid rocket motor; the remaining failures concerned liquid propellant rocket engines (LPREs). Within LPRE failures, the feeding system, pipes, valves and thrust chamber constitute 76% of cases, as shown in Figure 1.3.

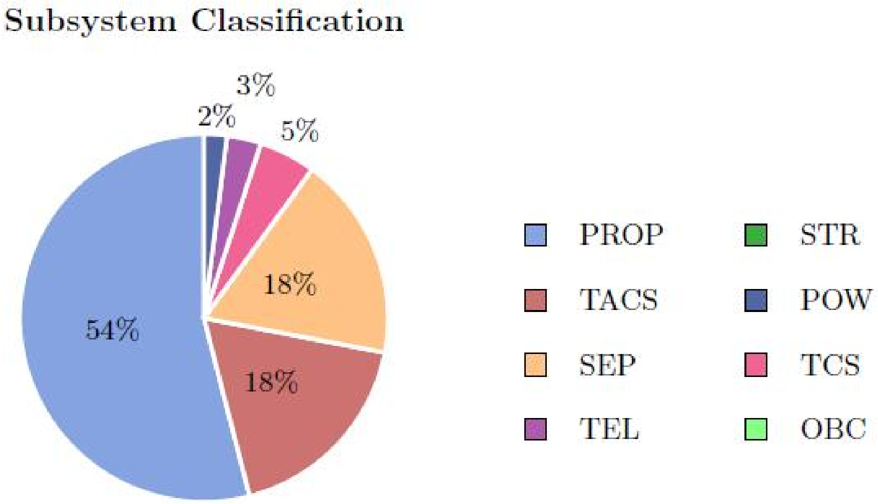

Figure 1.2: Launch Failures in the 15 years up to 2021 [1]

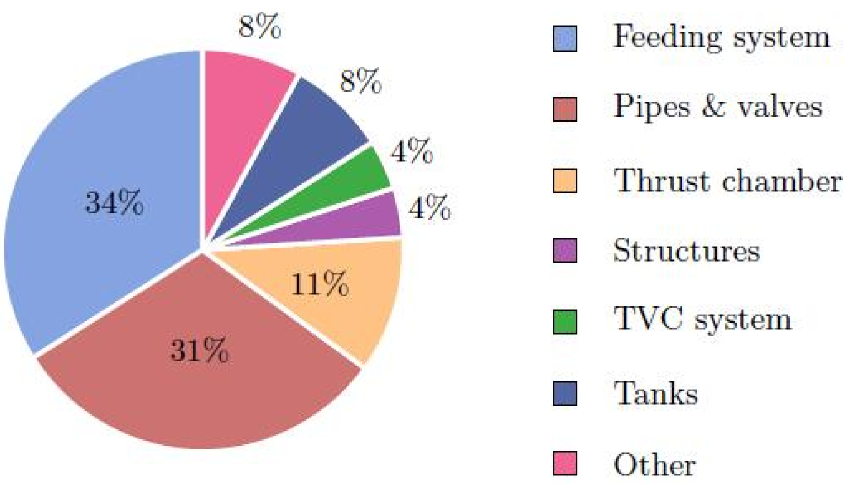

Figure 1.3: Launch Failure Roots in LPRE [1]

1.2 Scope of Thesis

The primary objective of this thesis is to develop a static (steady-state) performance model to support the preliminary design phase for a gas generator-cycle liquid-propellant rocket engine (LPRE). The model is a zero-dimensional tool that generates LPRE performance maps, enabling propulsion designers to trace engine performance throughout development and to related subsystem requirements directly to propulsion behaviour. Given that propulsion accounts for a high share of launch-vehicle failures, the thesis emphasizes establishing consistent, high-reliability requirements and deriving clear performance relationships among propulsion subsystems.

In order to establish such requirements, the physics of complex LPREs must be modeled. The developed static model provides the engine performance outputs under varying propellant flow rates (e.g., gas generator oxidizer flow rate, thrust chamber fuel flow rate) and hydraulic resistances (e.g., gas generator oxidizer control valve position). During subsystem development, individual components may deviate from expected performance. The performance tool evaluates how such deviations affect the engine's performance outputs and provides responses at all engine station points.

The approach is computationally efficient, delivering rapid and reliable predictions suitable for early design stages without the resource demands of high-fidelity transient simulations. The model covers turbopumps, piping, valves, cooling channels, injectors, the gas generator and the thrust chamber. It computes performance for any change in system parameters. Thus, off-design performance maps can be produced.

The ultimate goal is to enhance the preliminary design process by enabling a comprehensive analysis of subsystems relationships, reducing schedule risk when critical decisions must be made and contributing to LPRE technology.

2. LITERATURE REVIEW AND BACKGROUND

2.1 Liquid-Propellant Rocket Engine Cycles

Liquid-propellant rocket engines have different system architectures and cycles, but all ultimately delivery propellants from the tanks to the thrust chamber at the required flow rate, pressure and temperature. Thrust is generated by releasing the chemical energy of fuel and oxidizer mixture in the thrust chamber. In LPREs, propellant pressurization is performed either by pressurized gas (pressure-fed) or by turbomachinery (pump-fed). Liquid-propellant rocket engines can be mainly classified into pressure-fed, gas-generator cycle (open) cycle, staged-combustion cycle, expander cycle and electric pump-fed cycle. Each system architecture has advantages and disadvantages relative to the others.

In LPREs, the Pressure-fed engines have the simplest feed system. The engine uses propellant tanks pressurized by a high-pressure pressurant gas (typically helium or nitrogen) and deliver propellants to the thrust chamber through regulators, lines, and valves. To maintain the required pressure drop across the feed system and injectors, tank pressure must exceed chamber pressure, so the tanks are built heavier to withstand the higher pressure. This leads to heavier tank designs. The absence of turbomachinery reduces complexity, however, the achievable chamber pressure and thrust are limited by tank mass and pressurant requirements. Consequently, pressure-fed engines typically have lower thrust and, often, lower specific impulse than comparably sized pump-fed engines. Theese engines are mostly used in small launchers, upper stages, and attitude-control applications. Figure 2.1 shows a schematic of pressure-fed liquid-propellant rocket engine

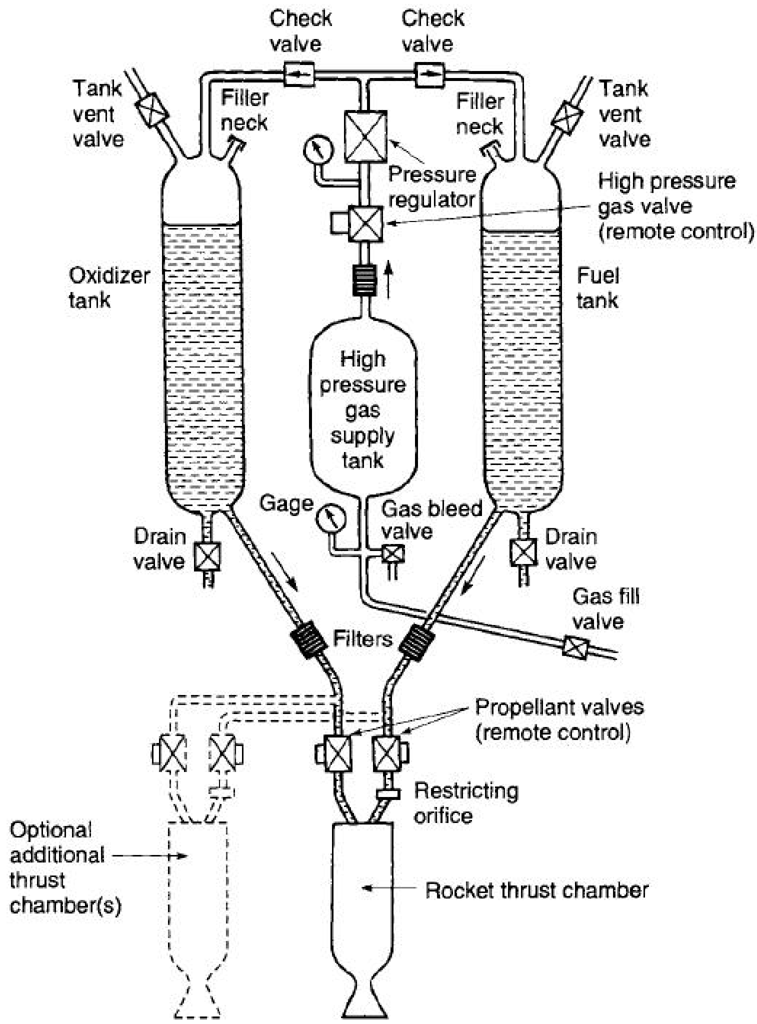

Figure 2.1: Pressure-fed system schematic [2]

Gas generator-cycle liquid-propellant rocket engines are open-cycle and have turbomachinery. In gas generator-cycle LPREs, there are oxidizer and fuel pumps hat pressurize the propellants. The turbine produces the work required to drive the pumps. In order to produce work in the turbine, high entalphy gas is needed, and this gas is produced in the gas generator. A small portion of the total propellant (generally between 3-7% of the total) is burned in the gas generator [3] and the remaining propellant is burned in the thrust chamber to produce thrust. The hot gas produced in the gas generator drives the turbine and this gas is dumped overboad after the turbine. Therefore, the specific impulse is lower than that of other closed-cycle liquid-propellant rocket engines. Figure 2.2 shows a typical gas generator-cycle engine.

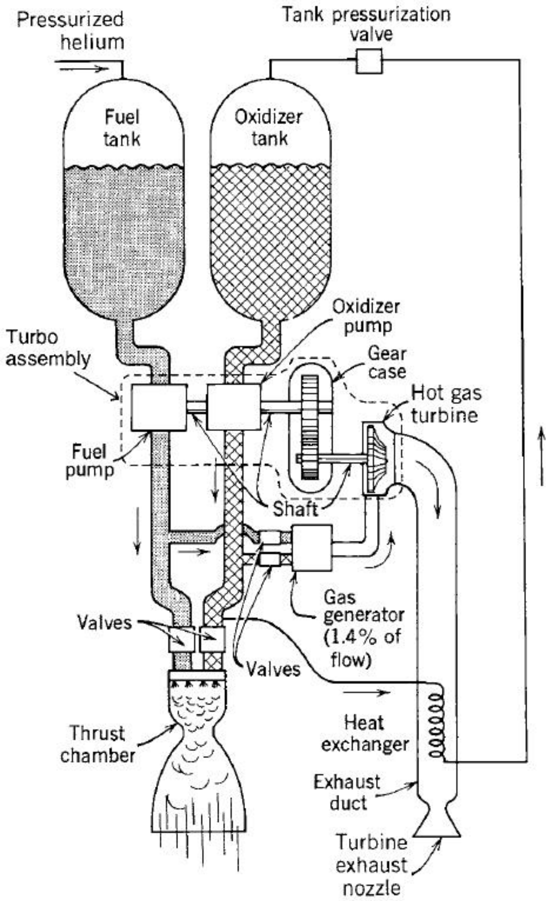

Figure 2.2: Gas generator cycle engine schematic [2]

Many gas generator cycle LPREs have been developed by different countries. For the Apollo missions, the F-1 engine was developed and used in the first stage of the Saturn V launch vehicle. Figure 2.3 shows the first stage of Saturn V, and the engine used in this vehicle is still the most powerful single-chamber rocket engine [3].

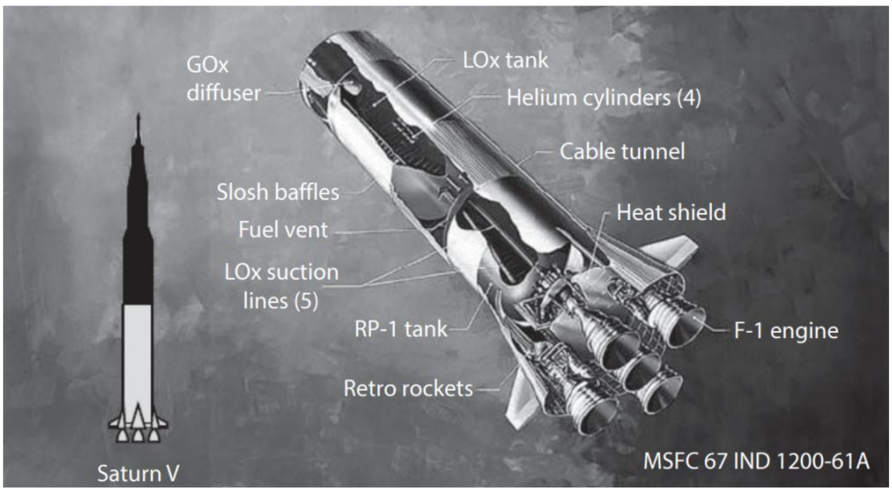

Figure 2.3: First Stage of Saturn V [3]

In recent years, in United States, SpaceX has a developed a gas-generator cycle LPRE, and a notable example is the Merlin engine family, known for its high thrust-to-weight ratio [4]. Figure 2.4 shows a Merlin 1D engine firing test.

Figure 2.4: Merlin 1D [4]

The CE-20 was developed by the Indian Space Research Organization (ISRO) and is used in the upper stage of the Launch Vehicle Mark-3 (LVM3) [5]. Figure 2.5 shows the CE-20 engine piping and instrumantation diagram (P&ID).

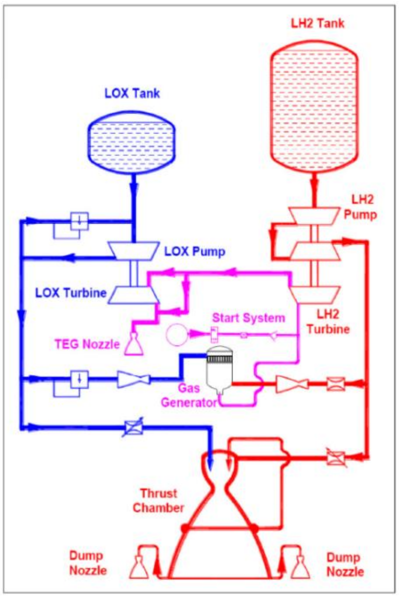

Figure 2.5: CE-20 P&ID [5]

The L75 engine has been under development at the Instituto de Aeronautica e Espaço (IAE) as Brazil’s first project to design and build an open-cycle LPRE [6]. Figure 2.6 shows the L75 P&ID.

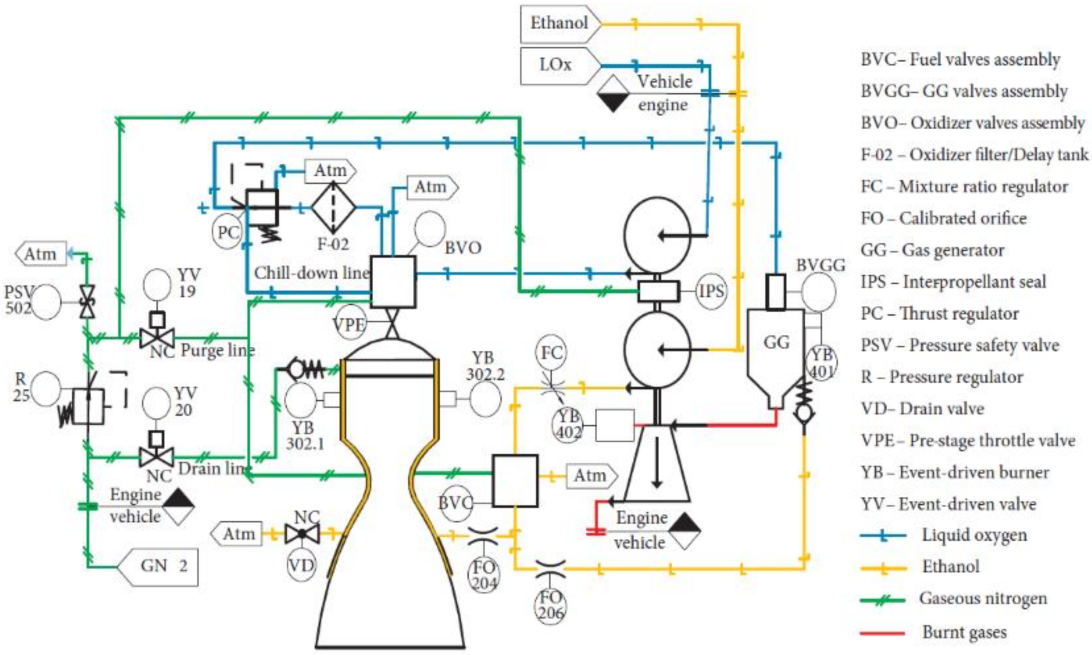

Figure 2.6: L75 P&ID [6]

The Korean Aerospace Research Institute (KARI) has developed sounding rockets and launch vehicles. Figure 2.7 presents the historical development of sounding rockets and launch vehicles by KARI.

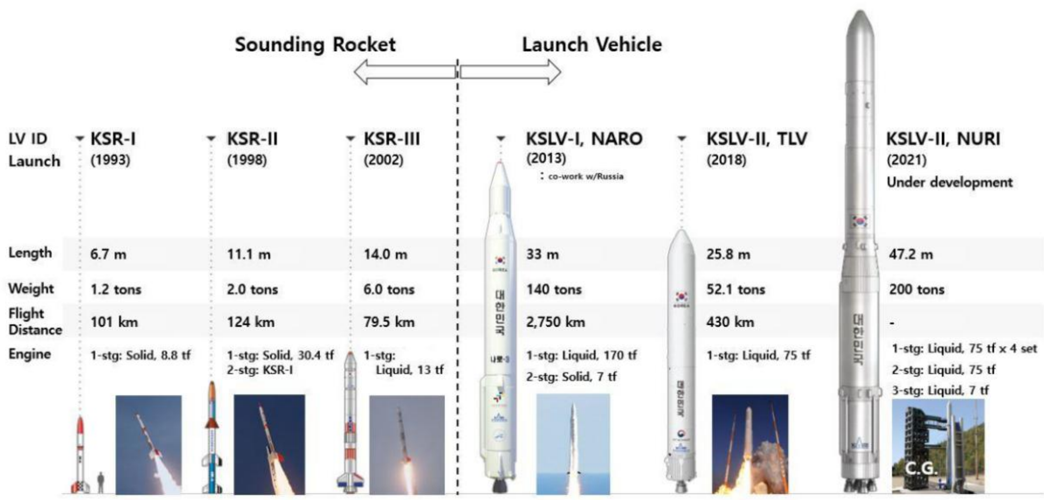

Figure 2.7: Sounding Rockets and Launch Vehicles developed by KARI [7]

Based on the technology developed for the 30-tonf LPRE, a 75-tonf LPRE was developed. This engine is used on the first stage of the the Korean Space Launch Vehicle – II (KSLV-II), and its vacuum variant is used on the second stage of the KSLV-II. Figure 2.8, Figure 2.9 show the P&ID and design of the 75-tonf LPRE on the first stage of KSLV-II.

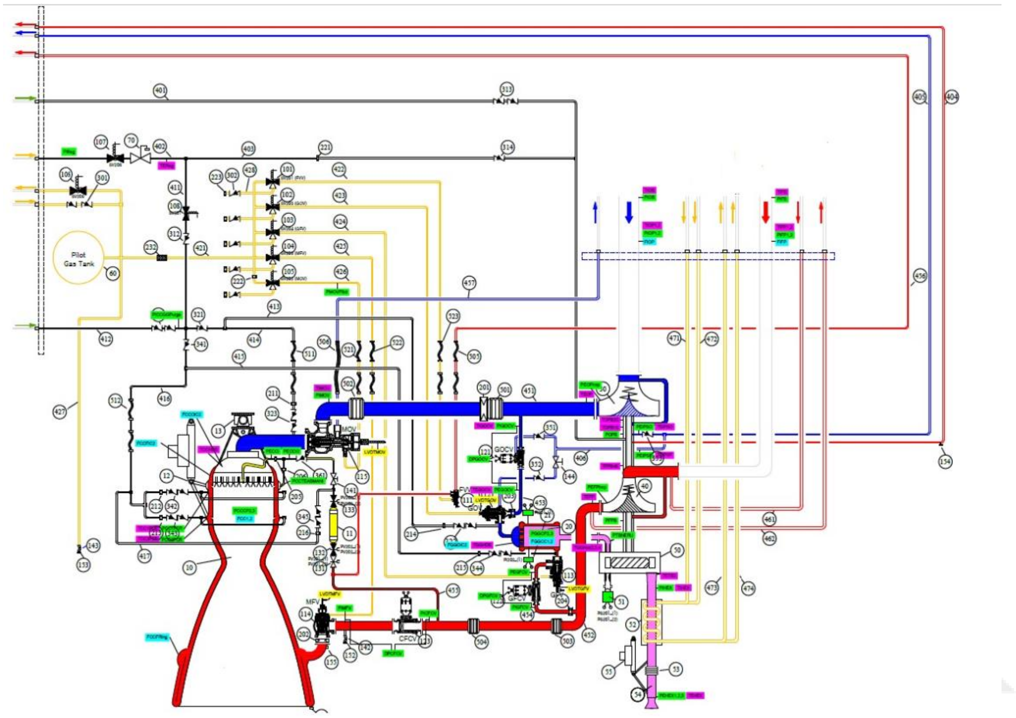

Figure 2.8: KRE-075 LPRE detail P&ID [8]

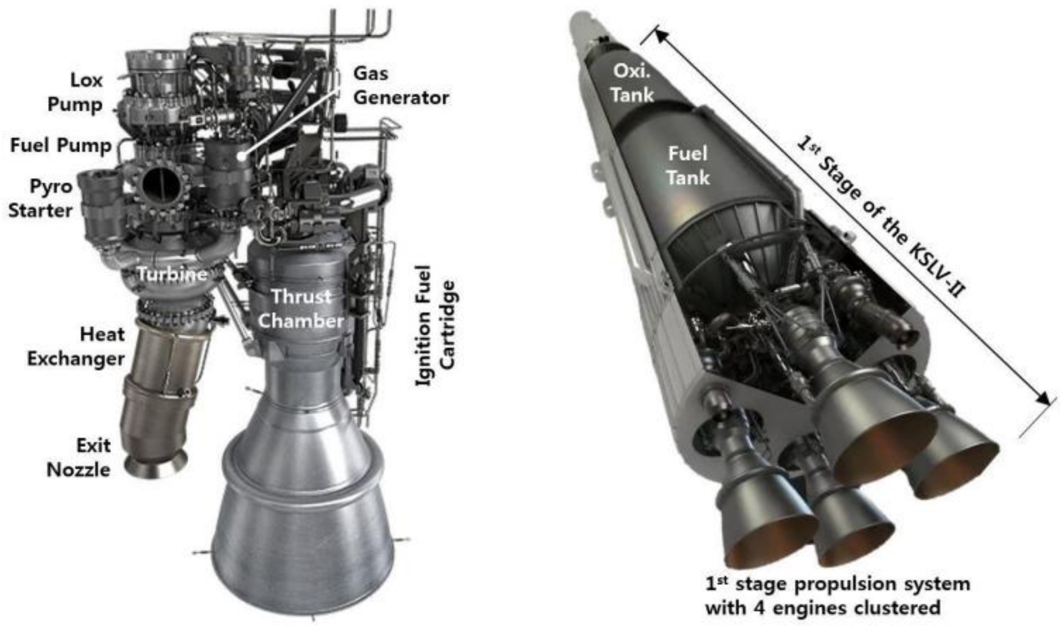

Figure 2.9: 75-tonf LPRE and first stage of KSLV-II [7]

The staged-combustion cycles are more efficient compared to gas generator-cycle LPREs. However, their complexity is higher than that of GG-cycle LPREs. Staged-combution cycle engines are closed cycles. There is a preburner instead of a gas generator, the preburner produces the hot gas to drive the turbine. Unlike the gas generator cycle, the turbine exhaust gas is not vented to the atmosphere. Instead, the turbine exhaust gas is fed into the main combustion chamber; thus, all propellants contribute to the thrust produced in thrust chamber.

There are three main staged-combustion cycles which are oxidizer-rich staged combustion cycle, fuel-rich staged combustion cycle and full-flow staged combustion cycle.

If the preburner is designed for oxidizer-rich combustion, the cycle is called oxidizer-rich staged combustion cycle. This approach is commonly observed in Russian LPREs; RD-180 engine uses an oxidizer rich staged combustion cycle [2].

Instead of preferring oxidizer-rich combustion in the preburner, the fuel-rich staged combustion cycle uses a fuel-rich preburner. These engines are commonly designed in the United States; the most well-known example is the RS-25 engine for National Aeronautics and Space Administration (NASA) Space Launch System (SLS) [2]. Figure 2.10 illustrates a schematic of fuel-rich staged combustion cycle.

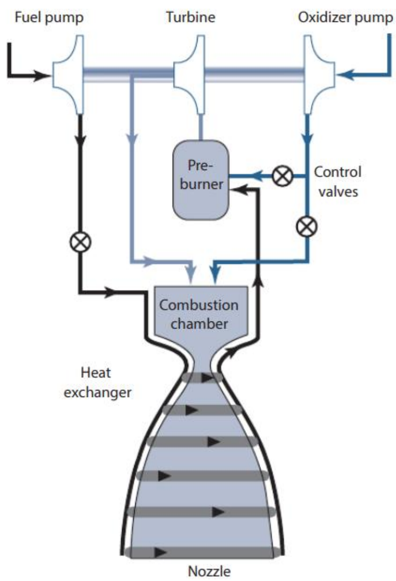

Figure 2.10: Fuel-rich staged combustion cycle schematic [3]

There are two preburners in the full-flow stage combustion cycle, one fuel-rich and the other oxidizer-rich. Figure 2.11 shows a full flow staged combustion cycle schematic.

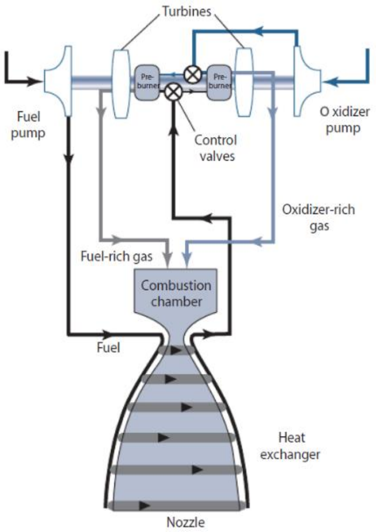

Figure 2.11: Full flow staged combustion cycle schematic [3]

The SpaceX Raptor engine that used on the Starship and Super Heavy Launch Vehicles, uses a full flow stage combustion cycle [3].

In expander-cycle LPREs, the required turbine drive working gas is obtained from the combustion chamber's cooling channels. Fuel is heated, vaporized as heat transferred from the combustion chamber walls along the cooling passages. The heated fuel drives the turbine. If the turbine exhaust gas is fed into the combustion chamber, the cycle is a closed expander cycle, as shown in Figure 2.12.

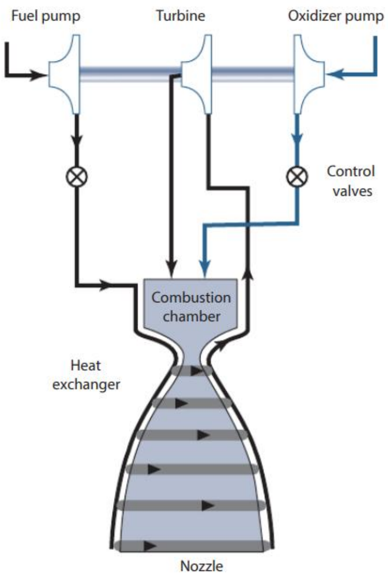

Figure 2.12: The closed expander cycle schematic [3]

In another type of the expander cycle, a small portion of the propellant is used to drive the turbine, and this portion is dumped overboard after the turbine. Figure 2.13 shows a schematic of an open expander cycle LPRE schematic. The specific impulse is lower than that of closed cycle expander LPREs, because of the overboard flow.

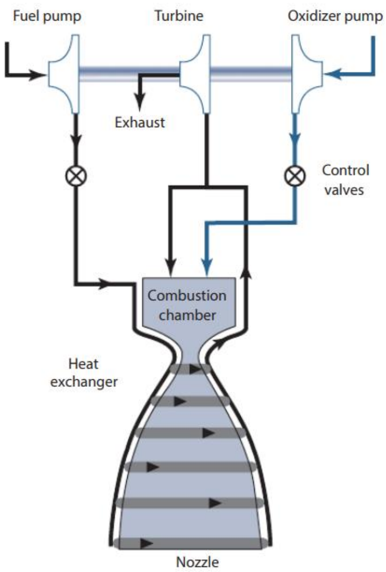

Figure 2.13: The open expander cycle LPRE schematic [3]

Electric pump fed LPREs use electrically powered pumps; therefore, a high enthalpy gas generation system is not required. Batteries provide the power required by the pumps. Figure 2.14 illustrates a schematic of an electric pump-fed LPRE.

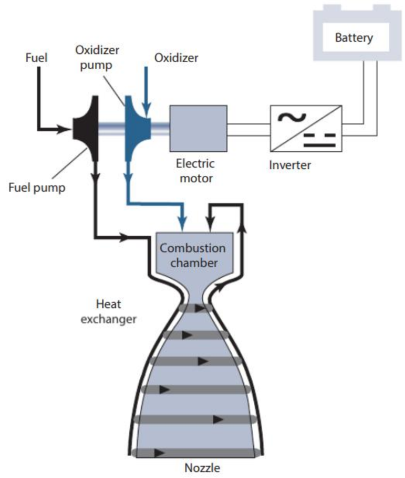

Figure 2.14: Electric pump-fed LPRE schematic [3]

2.2 Liquid Propellant Rocket Engine Performance Modelling: Methods and Trends

A lot of modeling studies of LPRE have been conducted to support LPRE development and reduce development costs. In the literature, LPRE modeling studies are commonly classified as zero-dimensional (0D), one-dimensional (1D) and three-dimensional (3D).

Three-dimensional (3D) computational fluid dynamic (CFD) analyzes and models are applied at the component level such as injector elements, cooling channels and turbomachinery flow paths. These analyses provide high fidelity, but their computational cost is high. Therefore, this approach is generally not feasible for full engine simulation.

1D network analyses are primarily developed and performed to model transient effects. In this context, the well known tools are GFFSP, ROCETS, RPA and EcosimPro.

ROCETS (Rocket Engine Transient Simulation) was developed for NASA by Pratt & Whitney. This program provides 1D transient and steady-state analyses, using 24 component modules (e.g., combustion chamber, pump), 57 sub modules [9].

Binder modeled RL10A-3-3A rocket engine using the ROCETS software and he compared simulation results with test data. The steady-state model predictions were found to be more accurate than the transient model results. For all measured data, steady-state results were within about 4% error range. In transient calculations, most results were within 4% error, whereas the turbine inlet temperature differed by up to 7%. Binder indicated that the discrepancy between the steady-state and transient calculations was caused by cooling jacket heat transfer modeling. Steady-state calculations use a heat transfer model based on test data, whereas the transient model relies on more complex theoretical calculations [10].

GFSSP (Generalized Fluid System Simulation Program) was also developed by the NASA and provides 1D transient and steady-state analyses to derive flow rates, pressures, temperatures and concentrations in a complex flow network. GFSSP is implemented using the finite volume formulation of the mass, momentum and energy conservation equations with equations of state for real fluids [11]. This tool is typically used for specific transient cases such as water-hammer and chilldown rather than for modeling a full engine simulation. Access to and use of ROCETS and GFSSP are subject to government approval.

EcosimPro is a zero-dimensional and one-dimensional simulation tool developed by Empresarios Agrupados. This tool also supports optimization and parametric studies. It is not dedicated solely to modeling LPREs; it is also used across hydraulic, pneumatic, thermal, mechanic and control domains to solve multidisciplinary engineering problems. Systems can be modeled in 0D and 1D form, and their behavior can be analyzed under both steady-state and transient conditions. For space propulsion applications, EcosimPro offers the European Space Propulsion System Simulation (ESPSS) libraries developed in collobration with European Space Agency (ESA) to model rocket and satellite propulsion systems. Access to ESPSS module is subject to ESA pre-approval [12].

Park, S., Lee, E. and Lee, M studied one-dimensional gas generator cycle LPRE model in EcosimPro and they performed a Monte Carlo analysis using 500 run simulations. Thus, they quantified how component level tolerances propagate to system performance. They varied the total dynamic heads of oxidizer and fuel pumps, pumps and turbines efficiencies, turbine nozzle and thrust nozzle diameters, and evaluated their effects on main chamber pressure, main chamber mixture ratio, turbine inlet temperature and nozzle thrust. They claim that the Monte Carlo approach gives a narrower range of output variations than room sum square (RSS) analysis and it is more efficient for designing gas generator cycle LPRE [13].

DLR (Deutsches Zentrum für Luft- und Raumfahrt e.V.) has developed an in-house tool that analyzes the performance of the main components and calculates the engine power balance and overall engine performance. There is no publicly available information about this tool or its algorithmic structure. Therefore, the details of the underlying mathematical model and the scope of the tool remain unknown [14].

1D network analyzes models are more accurate compared to zero-dimensional models. However, solution time is higher. Therefore, when the change is needed in the some parameters to shifting system from one point to another point, more quick solution method is needed. With this purpose, some methodologies were studied for preliminary design stages of LPRE.

Park, S.Y. and Cho, W.K. studied a program which solves 13 independent equations to calculate 13 independent variables to perform mode analysis of gas generator cycle LPRE. In this study, Newton method is used to solve equations numerically. Then, they calculated other engine performance parameters using found 13 variables. They showed the effect of change in gas generator oxidizer pressure change due to increasing loss coefficient of control valve. They indicated that gas generator oxidizer mass flow rate is reduced and this leads to decreasing turbopump rpm and combustion chamber pressure [15].

Cho, W.K. and Park, S.Y. analyzed a gas generator cycle LPRE without active control to demonstrate how propellant supply conditions affect system performance. They used a model that solves 13 independent equations for 13 engine variables, following algorithm shown in Figure 2.15. After validating the model with tests, they performed sensitivity studies on propellant density and inlet pressure. They reported that increasing oxidizer supply pressure raises the main performance parameters such as flow rates, turbopump speed, chamber pressure, whereas increasing fuel supply pressure has a limited overall effect because the higher fuel flow shifts the gas generator mixture ratio to the fuel rich side and reduces turbine power. They also found that higher oxidizer density increases chamber pressure, and higher fuel density increases chamber pressure since the total mass flow rate increases [16].

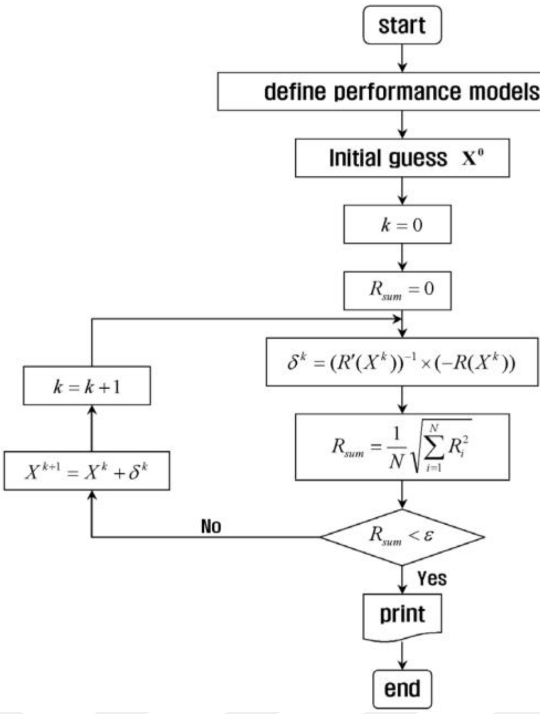

Figure 2.15: Solution algorithm for the coupled engine equations [16]

Cho, W.K. and Kim, C. analyzed how pressure drops in the feed lines of gas generator cycle Liquid Oxygen (LOX) / Kerosene LPRE affect performance. They used a mode analysis model that solves 15 independent equations to obtain 15 engine variables. The study varied pressure losses in four main lines including combustion chamber oxidizer and fuel lines, gas generator oxidizer and fuel lines. They examined the effects on turbopump speed, chamber pressure and gas generator temperature. They found that changes in combustion chamber oxidizer line and gas generator feed lines are the main drivers of turbopump RPM. Also, gas generator oxidizer line having the strongest influence, while the combustion chamber fuel line has the weakest effect on turbopump RPM. It was also stated that the changing pressure drop in the gas-generator lines alters thrust almost twice as effectively as changes in the combustion chamber lines. The pressure drop adjustments in the combustion chamber feed lines can be used to tune the chamber mixture ratio [17].

3. MATHEMATICAL MODELLING OF GAS GENERATOR CYCLE LIQUID PROPELLANT ROCKET ENGINE

3.1 Gas Generator Cycle Liquid Propellant Rocket Engine

Gas generator cycle LPRE mainly consists of oxidizer, fuel pumps, hydraulic lines, flow control valves, cooling channels in thrust chamber and gas generator, thrust chamber and gas generator injectors, turbine and turbine exhaust system. Depending on system design, some differences may observed in these systems. For instance, some gas generator cycle liquid propellant rocket engines have passive control elements on the hydraulic lines such as orifices, cavitating venturi, and in some rocket engines there are active control elements such as mixture ratio control valve, thrust control valve. On the other hand, turbine exhaust systems can differ one by one. In some systems, especially in cryogenic systems, pressurizing system has heat exchanger and this is located generally in turbine exhaust. Using high temperature gaseous, cryogenic inert gaseous is heated and used for pressurizing tanks. Also, depending on propellant selections, some systems have to use ignition system. In hypergolic propellants, ignition systems are not needed but for nonhypergolic propellant it is needed.

3.1.1 Thrust chamber

The thrust chamber is a unit where chemical energy is produced from the fuel and oxidizer reaction and chemical energy is converted into kinetic energy and thrust by accelerating the high enthalpy gases through convergent-divergent nozzle. It comprises the injectors, the combustion chamber, the thermal coating or cooling systems and ignition system (if it is required), nozzle for gas expansion and structural elements that transmits thrust loads.

Injector provides atomization of oxidizer and fuel, and droplets are occurred in combustion chamber. Droplets are vaporized since these absorb heat from the hot environment. The mixed gases continue heating; once ignition criteria are met, combustion proceeds. In chambers with stable combustion, complete vaporization and reaction of the propellants are expected within the region upstream of the throat.

The thrust chamber is a unit where chemical energy is released from the fuel and oxidizer reaction, then, chemical energy is converted into kinetic energy and thrust by accelerating the high entalphy gases through convergent divergent nozzle. It comprises the injectors, the combustion chamber, the thermal coating or cooling systems and ignition system (if it is required), nozzle for gas expansion and structural elements that transmits thrust loads.

Injectors atomize of oxidizer and fuel, and droplets are formed in combustion chamber. These droplets absorb heat from the hot environment and vaporize. Vaporized droplets are mixed and these mixed gases continue heating; once ignition/activation criteria are met, combustion proceeds. In chambers with stable combustion, complete vaporization and reaction of the propellants are expected within the region upstream of the throat.

In order to calculate performance of thrust chamber, mostly used specific impulse term which indicates the thrust per mass flow rate. Specific impulse is affected by combustion efficiency of propellants, product gas expansion performance in nozzle, oxidizer and fuel ratio and atomization efficiency [18].

$$I_{sp} = \frac{F}{\dot{m}} \tag{3.1}$$

Characteristic velocity is another performance parameter which indicates combustion performance [18].

$$c^* = \frac{P_{cc} A_{throat}}{\dot{m}} \tag{3.2}$$

Thrust coefficient is a measure of nozzle design quality and gas expansion properties [18].

$$C_f = \frac{F}{P_{cc} A_{throat}} \tag{3.3}$$

Thrust can be calculated as the sum of two terms: the momentum thrust and the pressure thrust. Momentum thrust is the mass flow rate multiplied by the exhaust velocity relative to the vehicle. Pressure thrust is the nozzle exit area multiplied by the pressure difference between the nozzle exit and the ambient.

$$F = \dot{m} v_{exhaust} + (p_{nozzle\_exit} - p_{ambient}) A_{nozzle} \tag{3.4}$$

Properties of the combustion products formed in the combustion chamber play a critical role in the thrust chamber performance calculations. These properties depend on chamber pressure and mixture ratio. In practice, these properties are often obtained by NASA's Chemical Equilibrium and Applications (CEA) that was developed at NASA Lewis Research Center. CEA computes the equilibrium composition and calculate thermodynamic properties of product gas based on minimizing Gibbs free energy. Thus, thermophysical data is provided for product gas such as viscosity, specific heat, average molecular weight. CEA uses propellant combination, combustion chamber pressure, mixture ratio, nozzle expansion ratio as input. Using these inputs, CEA computes gas properties along the nozzle and returns theoretical performance metrics including specific impulse I_{sp} and thrust coefficient C_f [19].

Using the theoretical specific impulse and thrust from CEA, the ideal mass flow rate can be computed as indicated in (3.5).

$$\dot{m}_{ideal} = \frac{F_{ideal}}{I_{sp_{ideal}}} \tag{3.5}$$

CEA results are theoretical. In practice, deviations arise from effects such as heat transfer and friction losses. To account for these effects, the literature uses correction factors. The first is the thrust coefficient correction that is the ratio of actual to ideal thrust, typically 0.92–1.00. A second factor corrects specific impulse and this correction factor is typically 0.85–0.98. Similarly, correction factors for mass flow rate and characteristic velocity are used as 0.98 –1.15 and 0.87 –1.03, respectively [18].

3.1.2 Gas generator

Gas generator's purpose is to produce the high enthalpy working gas that drives the turbine. It comprises the injectors, combustion chamber, the thermal coating or cooling systems and ignition system (if it is required). It has no expansion nozzle, and flow chocking occurs in the turbine rather than gas generator itself. Accordingly, the gas generator is designed to satisfy required mass flow, pressure and temperature to turbine rather than to obtain thrust. Nozzles are not located in the gas generator, nozzle placed in turbines. The mass flow rate chocking is occurred in turbine nozzles.

Gas generator temperature is a critical constraint. To avoid exceeding turbine operating limits, gas generator produced gas temperature must remain within allowable limits. Some gas temperature values for selected engines are given in Table 3.1.

Table 3.1: Different Engine Gas Generator Temperature Values [20, 21, 22]

Engine	Cycle	Propellant Combination	Gas Temperature (K)
F-1	GG	LOX / RP1	1062
KRE-075	GG	LOX / Jet A-1	900
RD-180	SC	LOX / Kerosene	820

Table 3.1 shows that the gas produced in the gas generator is not a stoichiometric condition. It is either very fuel or very oxidizer rich condition. For instance, the gas generator of the KRE-075 uses a mixture ratio of 0.321 (fuel-rich), whereas the RD-180 pre-burner operate at mixture ratio of 50 approximately [21, 22].

In highly fuel rich environments, the use of CEA is not appropriate. In a study performed in DLR, it is stated that CEA calculates higher temperature than the experimental results. With the cracking of long hydrocarbon chains; less hydrocarbon, pure carbon and hydrogen molecules are released in CEA results than the real. However, in fuel rich combustions, there are still unburned chain molecules. Figure 3.1 shows the deviation of combustion temperature value at lower mixture ratios [23].

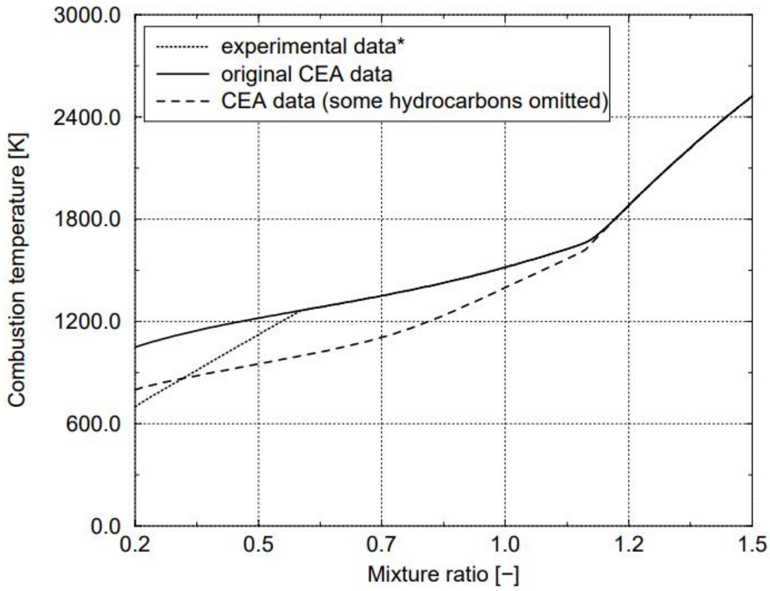

Figure 3.1: LOX – Kerosene combustion in fuel rich environment [23]

When surveying the literature, Huzel reports tabulated gas properties for low mixture ratio conditions. Table 3.2 summarizes these gas properties for LOX and Rocket Propellant-1 (RP1) [18]. Lee, S., Lim, T. and Roh, S.T. developed a subsystem based system analysis program for LPRE performance. Huzel's fuel – rich and oxidizer rich property sets were used in the gas generator module. Model results were compared to A-1 reference engine from Huzel, F-1 and RD-170. It was stated that specific impulse differences of about 1-2% and thrust to weight ratio deviations of smaller than 5%, which they judged to be within acceptable limits [24].

Table 3.2: Gas Properties for LOX / RP1 for Fuel Rich Mixture Ratio [18]

Temperature (K)	Cp	γ	R	Mixture Ratio (O/F)
866.4833	2658.618	1.097	232.96787574	0.308
894.2611	2675.3652	1.100	242.65245257	0.320

922.0389	2692.1124	1.106	253.41309348	0.337
949.8167	2704.6728	1.111	315.28677872	0.354
977.5944	2713.0464	1.115	271.16815098	0.372
1005.372	2725.6068	1.119	278.70059962	0.390
1033.15	2733.9804	1.124	288.38517644	0.408
1060.928	2742.354	1.128	298.06975326	0.425

Table 3.3 (continued): Gas Properties for LOX / RP1 for Fuel Rich Mixture Ratio [18]

Temperature (K)	**Cp**	γ	**R**	**Mixture Ratio (O/F)**
1088.706	2750.7276	1.132	312.05858645	0.443
1116.483	2759.1012	1.137	317.4389069	0.460
1144.261	2763.288	1.140	326.58545168	0.478
1172.039	2767.4748	1.144	335.73199645	0.497
1199.817	2771.6616	1.1448	344.34050918	0.516

In another study on LOX – Jet A-1 gas generators, the thermodynamic properties of the combustion products were modeled as functions of mixture ratio. The authors conducted fuel rich gas generator tests and compared the results with Huzel's tabulated data. They stated good agreement in gas temperature with Huzel's data, while gas constant (R), specific heat ratio (γ) and constant specific heat (C_P) were consistent with the values obtained from their interpolation correlations, as shown in Figure 3.2, Figure 3.3, Figure 3.4 and Figure 3.5 [25].

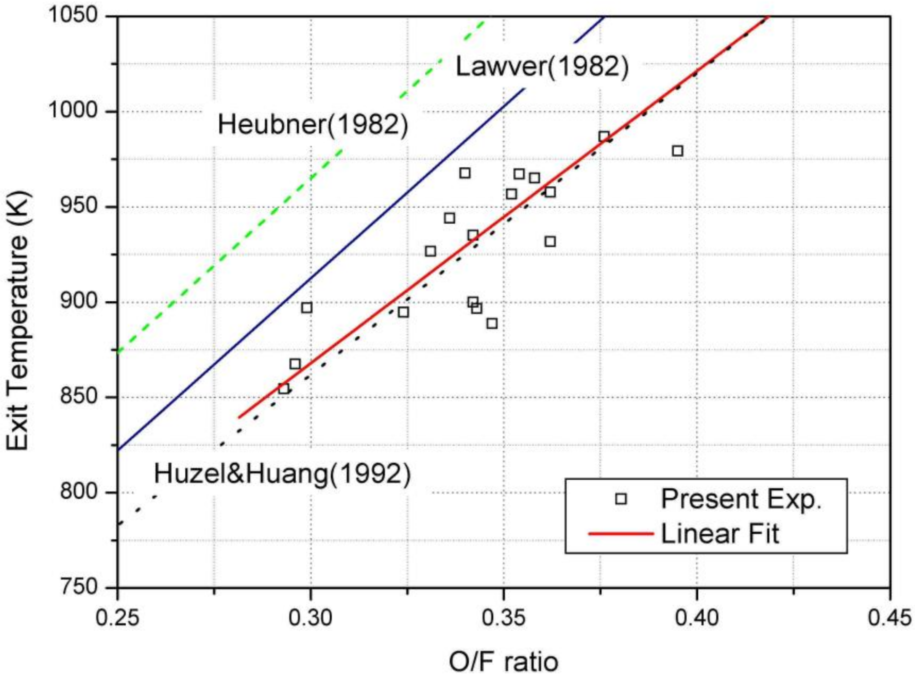

Figure 3.2: Temperature vs O/F ratio [25]

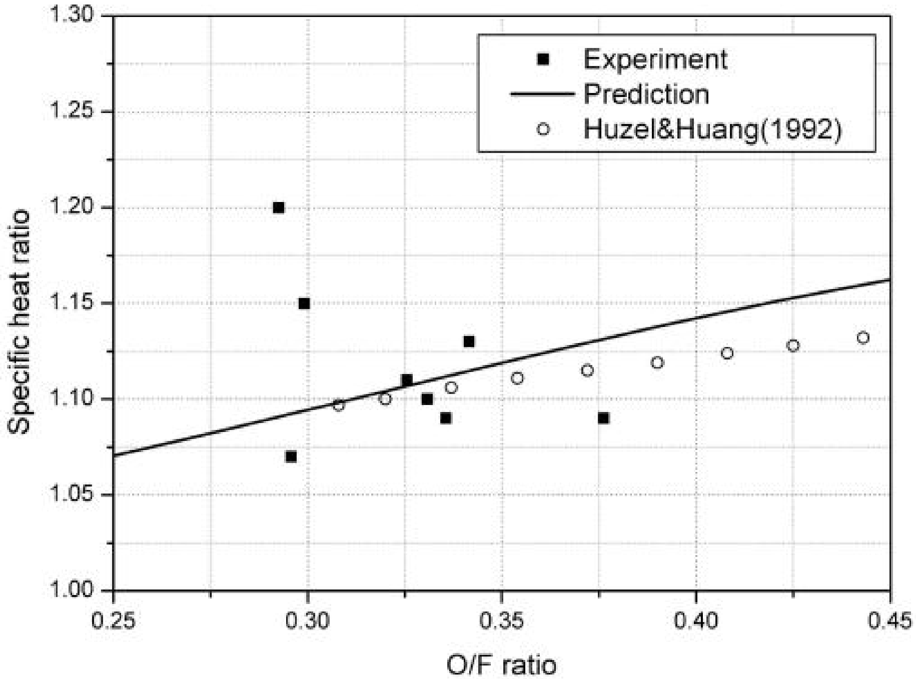

Figure 3.3: Specific Heat Ratio vs O/F ratio [25]

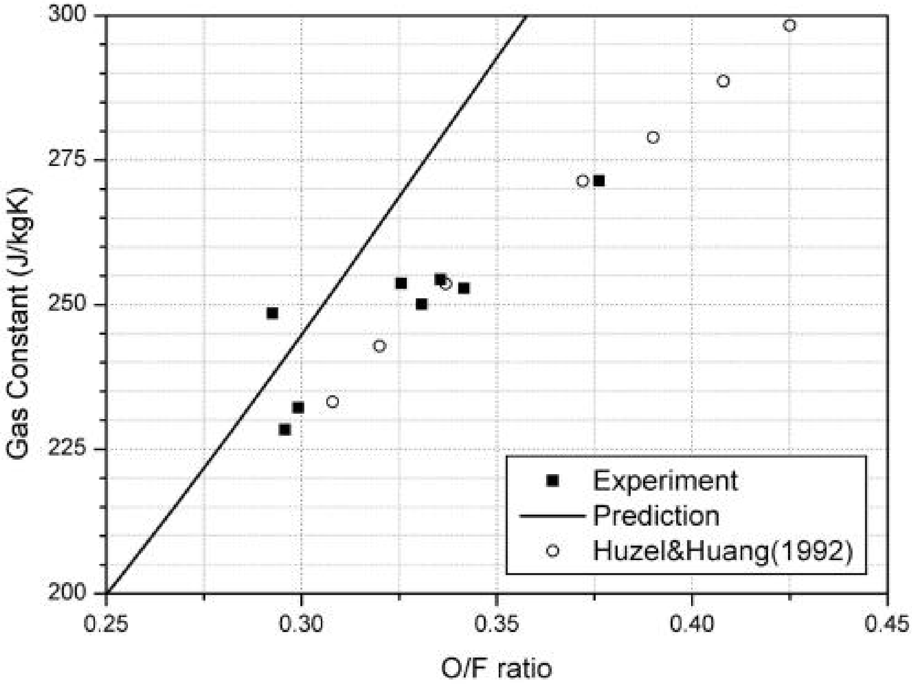

Figure 3.4: Gas Constant vs O/F Ratio [25]

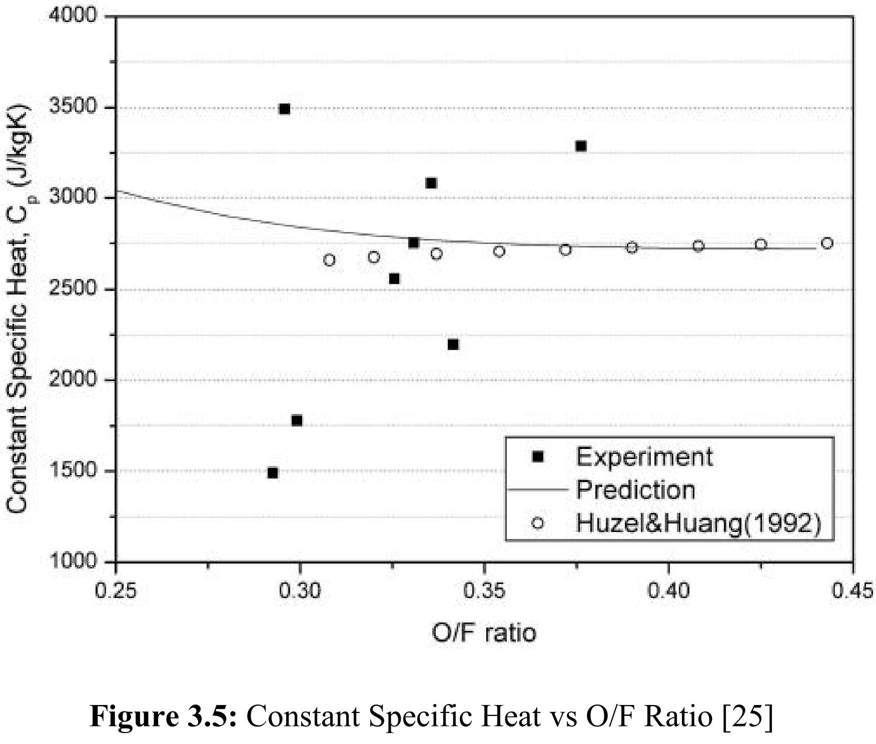

Figure 3.5: Constant Specific Heat vs O/F Ratio [25]

3.1.3 Injectors

Injectors atomize and deliver the propellants into the combustion chamber. Their design is critical for combustion efficiency because it influences the local mixture ratio, the droplet size distribution, and the droplet evaporation time. These parameters affect overall engine performance. For stable operation and to provide damping against instability, the injector is typically sized to impose a pressure drop on the order of 15 to 20 percent of chamber pressure. If the injector pressure drops falls to below about 5 percent of chamber pressure, chugging may occur [18]. There are many injector types, including impinging, swirl, dual manifold, high pressure drop, and pintle injectors. Different types affect the discharge coefficient and the stability characteristics. The pressure drop equation for injectors is given in the (3.6).

$$\dot{m} = C_d A_{inj} \sqrt{2\rho \Delta P} \tag{3.6}$$

3.1.4 Turbopump

A turbopump is an assembly that couples a turbine to one or more pumps to pressurize the propellants. Power produced by the turbine is transmitted to the pumps, which convert it into hydraulic power to raise propellant pressure and deliver the required flow to the engine. Various turbopump layouts appear in the literature, as presented in Figure 3.6. In the simplest arrangement, a single shaft carries the turbine and drives both the oxidizer and the fuel pump. Other architectures use separate turbines for each pump, or transmit turbine power through a gearbox that splits and matches power to the oxidizer and fuel pumps. These configuration choices are driven by required head and flow, rotational speed limits, packaging, and control strategy.

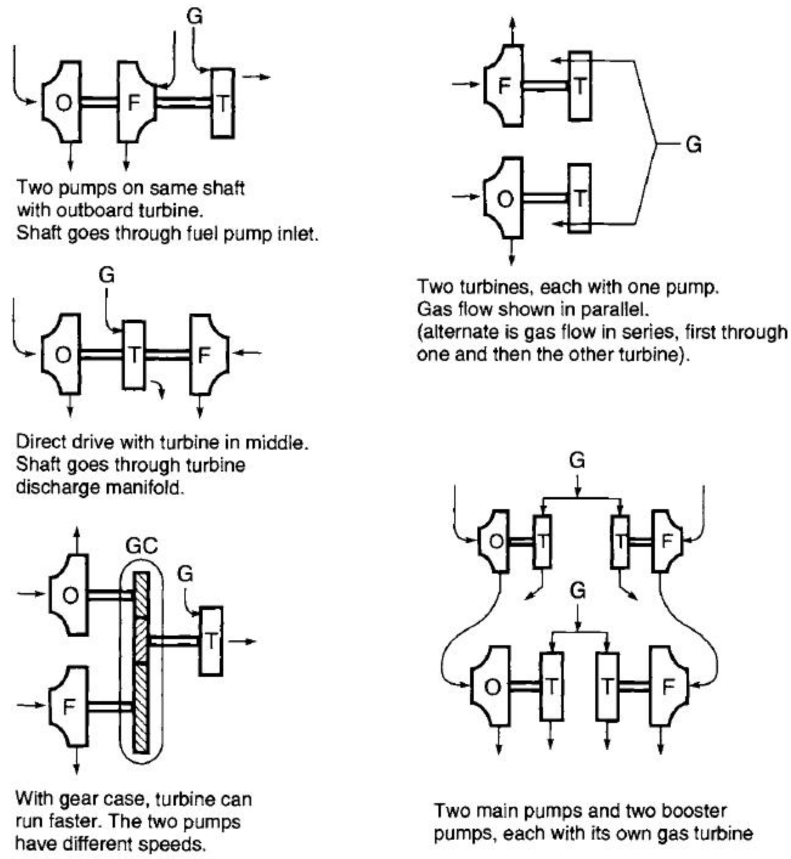

Figure 3.6: Different designs of turbopumps [2]

In a turbopump, the power produced by the turbine must equal the total power required by the pumps to pressurize the propellants.

$$\dot{W}_T = \dot{W}_{oxidizer\,pump} + \dot{W}_{fuel\,pump} \tag{3.7}$$

The head is commonly used to measure pressurization in the pumps. Head is defined as the pressure rise of the fluid divided by the product of the fluid density and the gravitational acceleration.

$$\Delta H = \frac{\Delta P}{\rho g_0} \tag{3.8}$$

The head generated by a pump depends on rotational speed and flow rate. It varies at different rpm and flow rate values. In an engine, the operating point is determined by the intersection of the pump characteristic curve and the system characteristic curve. Figure 3.7 shows a representative pump curve and the design operating point where it meets the system curve.

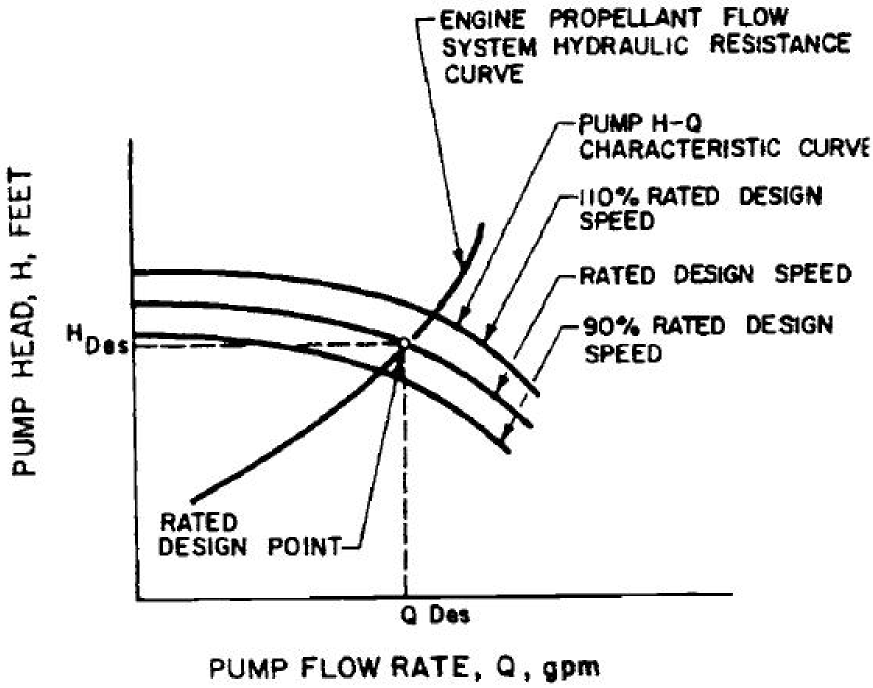

Figure 3.7: Pump characteristic curve and system hydraulic resistance curve [18]

The turbine must deliver slightly more than the sum of the pumps hydraulic power due to mechanical and hydraulic losses. Therefore, the pump power is calculated as indicated the Equation 3.9.

$$\dot{W}_P = \frac{Q\Delta P}{\eta} \tag{3.9}$$

Establishing the pump characteristic curves is essential for engine performance calculations. The common approach to testing pumps and construct to performance maps is to use dimensionless coefficients. In particular, the head coefficient (ψ) and the flow coefficient (Φ) enable derive pumps off design behavior. Thus, the head and efficiency can be obtained at different rotational speeds and flow rates.

$$\psi = \frac{gH}{N^2D^2} \tag{3.10}$$

$$\phi = \frac{Q}{ND^3} \tag{3.11}$$

Once the pump characteristic curves are derived, the head (or pressure rise) can be expressed as a function of rotational speed and flow rate. Cho, K. W. and Kim, C.

used the Equation (3.12) to calculate the pressure rise across the pump; the equation includes the rotational speed n, mass flow rate m , fluid density ρ and fitted coefficients calibrated to the pump curves.

$$\Delta P = A\rho n^2 + Bn\dot{m} + C\dot{m}^2/\rho \tag{3.12}$$

Analogous to the head correlation, pump efficiency can be modeled by regressing efficiency values against rotational speed and mass flow rate using the performance map. The resulting coefficients allow prediction at off-design conditions.

The turbine provides the power required by the pumps by using the working fluid's enthalpy. As the power produced by the turbine is converted to mechanical power, losses occur and are represented as efficiency in the work balance. The generated power depends on the enthalpy of the fluid and the mass flow rate. As the flow admitted to the turbine decreases, the overall system becomes more efficient.

$$\dot{W}_T = \eta_T \dot{m}_T (h_0 - h_e) \tag{3.13}$$

Under the ideal gas isentropic flow assumption, using the isentropic temperature and pressure relation, the turbine power equation is formed as indicated in the (3.14).

$$\dot{W}_T = \eta_T \dot{m}_T C_p T_0 (1 - (\frac{P_e}{P_0})^{\frac{\gamma-1}{\gamma}}) \tag{3.14}$$

Turbines can be designed as impulse or reaction types, as shown in Figure 3.8. In a reaction turbine, the gas expands as it passes through the rotor, and a pressure drop occurs across both the rotor and the stator nozzles. In an impulse turbine, most of the pressure drop occurs in the nozzles, and the rotor primarily converts the jet velocity into work. Reaction turbines are commonly used for low pressure ratios and high flow rates, whereas impulse turbines are preferred for high pressure ratios and low flow rates.

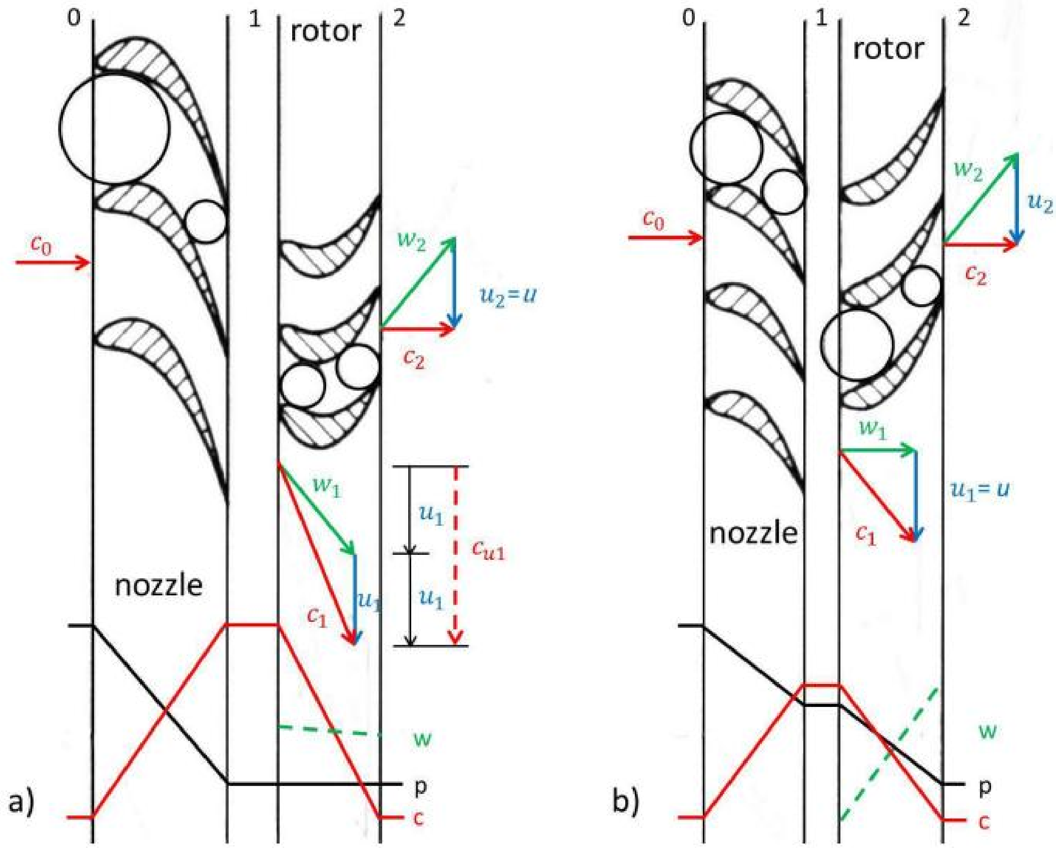

Figure 3.8: Impulse (a) and reaction type (b) [26]

The velocity corresponding to the isentropic enthalpy drop from the turbine inlet stagnation pressure to the final exhaust pressure is called the spouting (isentropic) velocity C_0.

$$C_0 = \sqrt{2C_pT_0[1-(\frac{p_e}{P_0})^{\frac{\gamma-1}{\gamma}}]} \tag{3.15}$$

Turbine efficiency varies with turbine types, stage count and ratio of the pitchline velocity U to the isentropic spouting velocity C_0 (U/C_0). Figure 3.9 shows a trend of efficiency versus these parameters as representative. In order to maximize energy extraction from the working fluid, a high turbine inlet temperature and a large pressure drop ratio are desirable which increase C_0. However, higher spouting velocity causes higher pitchline velocity. Because pitchline velocity is limited by centrifugal stresses, the turbine design can be different from the best efficieny point [27].

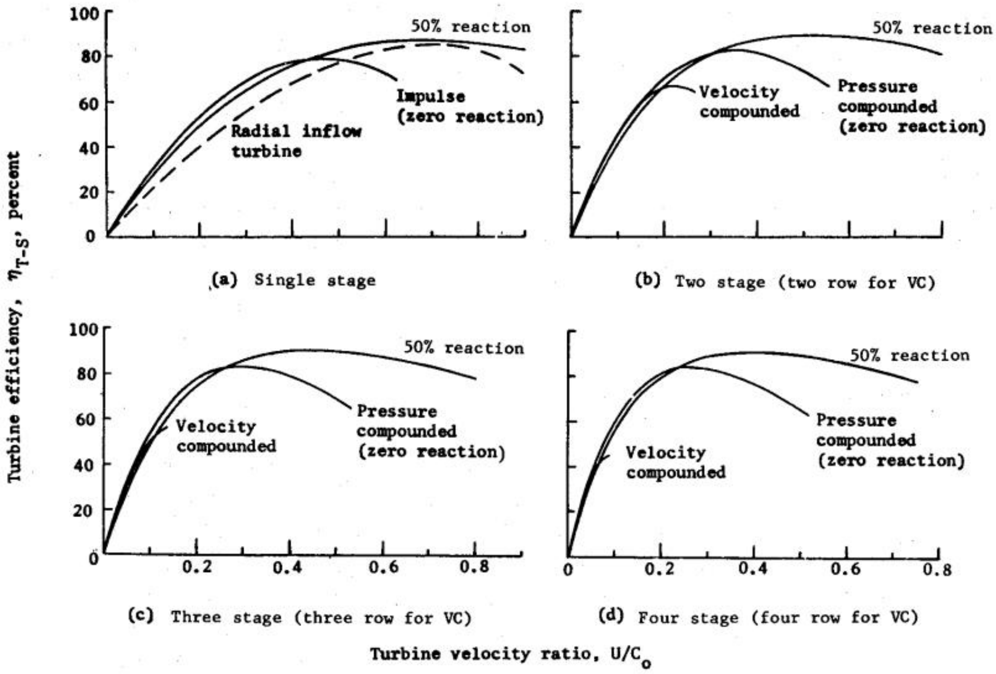

Figure 3.9: Turbine Efficiency for Different Designs [27]

Turbine performance map is established through a combination of high-fidelity analysis and experiments. Turbine efficiency can be expressed as function of rotational speed and pressure ratio. Thus, the turbine efficiency can be calculated for off-design operating conditions.

3.1.5 Valves & feed lines

The valves are used to isolation propellants to thrust chamber and gas generators. According to operation sequence, these are opened and propellants flows to combustion chambers. Not only shut off valves but also control valves are used in LPREs. The control valves are used to mixture ratio controlling or throttling.

The pressure drop calculations for valves and feed lines are not straightforward. These depend on material properties (e.g., roughness), diameter, inlet pressure which means the general analysis is not applicable.

The pipe loss can be calculated using (3.16) including density of propellant ρ, flow velocity V, and the flow coefficient K [24].

$$\Delta P = \frac{1}{2}\rho V^2 K \tag{3.16}$$

$$K = f\frac{L}{D_h} \tag{3.17}$$

The valve pressure drop is calculated using valve coefficient in practice. Valve coefficient (C_V) is determined with the experiments and this enables to calculate pressure drop [28].

$$\Delta P = \rho(\frac{Q}{C_v})^2 \tag{3.18}$$

4. STATIC PERFORMANCE TOOL

The static performance tool is a numerical model that determines sixteen key engine performance variables by solving sixteen coupled nonlinear equations simultaneously. Using obtained sixteen key performance parameters, all system performance parameters can be calculated. Sixteen unknown performance parameters are shown in $\vec{\boldsymbol{X}}$.sixteen nonlinear equation is solved as iteratively and $\vec{\boldsymbol{X}}$ is updated at each iteration. When residual values are converged to zero, $\vec{\boldsymbol{X}}$ is not updated and this $\vec{\boldsymbol{X}}$ is found as solution root.

$$\vec{X} = \begin{bmatrix} \textbf{turbopump rpm} \\ \textbf{TC LOx flow rate} \\ \textbf{TC Fuel flow rate} \\ \textbf{LOx Pump Outlet Pressure} \\ \textbf{Fuel Pump Outlet Pressure} \\ \textbf{TC Pressure} \\ \textbf{GG LOx flow rate} \\ \textbf{GG Fuel flow rate} \\ \textbf{GG Pressure} \\ \textbf{Turbine Adiabatic Velocity} \\ \textbf{Turbine Efficiency} \\ \textbf{Turbin Outlet Temperature} \\ \textbf{Turbine Exit Pressure} \\ \textbf{LOx Pump Efficiency} \\ \textbf{Fuel Pump Efficiency} \\ \textbf{Turbine Nozzle Exit Mach} \end{bmatrix}$$

The first two of sixteen equations are solved to obtain the head of the oxidizer and fuel pumps as functions of mass flow rate and rotational speed. The pump discharge pressures are then determined by adding the calculated head to the inlet boundary pressures $P_{tpi,o}$ and $P_{tpi,f}$. The coefficients A, B, and C in the equations are specific to the characteristic curves of the fuel and oxidizer pumps and differ for the two pumps.

$$R_1 = \underbrace{P_{tpe,o}}_{pump\ outlet\ pressure\ at\ i} - \underbrace{\left(\underbrace{P_{tpi,o}}_{inlet\ pressure} + \underbrace{A_{H,o}n_{tp}^2 + B_{H,o}n_{tp}\dot{m}_o + C_{H,o}\dot{m}_o{}^2}_{Head} \right)}_{calculated\ pump\ outlet\ pressure\ at\ i+1} \tag{4.1}$$

$$R_2 = \underbrace{P_{tpe,f}}_{pump\ outlet\ pressure\ at\ i} - \underbrace{\left(\underbrace{P_{tpi,f}}_{inlet\ pressure} + \underbrace{A_{H,f}n_{tp}^2 + B_{H,f}n_{tp}\dot{m}_f + C_{H,f}\dot{m}_f{}^2}_{Head} \right)}_{calculated\ pump\ outlet\ pressure\ at\ i+1} \tag{4.2}$$

The following three equations in the set derive the combustion-chamber pressure. Equations (4.3) and (4.4) compute the combustion chamber pressure by calculating the pressure losses along the hydraulic lines downstream of the oxidizer and fuel pump outlets.

Oxidizer is delivered from the oxidizer pump outlet and to the combustion chamber. Along this hydraulic path, the oxidizer passes the chamber oxidizer line, the chamber oxidizer valve, and the chamber oxidizer injector. The pressure loss across these hydraulic resistances must equal the difference between the oxidizer pump discharge pressure and the combustion chamber pressure.

$$R_3 = \underbrace{P_{tc}}_{thrust\ chamber\ pressure\ at\ i} - \underbrace{(\underbrace{P_{tpe,o}}_{pump\ outlet\ pressure} - \underbrace{\sum_i \Delta P_{components,i}}_{hydraulic\ pressure\ losses})}_{calculated\ thrust\ chamber\ pressure\ at\ i+1} \tag{4.3}$$

Similar to oxidizer hydraulic calculations, the pressure loss across the fuel hydraulic resistances must equal the difference between the fuel pump discharge pressure and the combustion-chamber pressure. Accordingly, the pressure drops are calculated along the combustion chamber fuel path includes combustion chamber fuel line and its components (e.g., orifices, valves, cooling channel, injectors.)

$$R_4 = \underbrace{P_{tc}}_{thrust\ chamber\ pressure\ at\ i} - \underbrace{(\underbrace{P_{tpe,f}}_{pump\ outlet\ pressure} - \underbrace{\sum_i \Delta P_{components,i}}_{hydraulic\ pressure\ losses})}_{calculated\ thrust\ chamber\ pressure\ at\ i+1} \tag{4.4}$$

The Equation (4.5) uses the fuel and oxidizer mass flow rates supplied to the combustion chamber and derives the combustion-chamber pressure. To determine the combustion-gas properties (γ, R, T) appearing in the equation, NASA's CEA ("Chemical Equilibrium with Applications") was used.

$$R_5 = \underbrace{P_{tc}}_{thrust\ chamber\ pressure\ at\ i} - \underbrace{\frac{\eta_{c^*}(\dot{m}_{tc,o} + \dot{m}_{tc,f})}{A_{n,tc}\sqrt{\frac{\gamma_{tc}}{R_{tc}T_{tc}}\left(\frac{2}{\gamma_{tc}+1}\right)^{\frac{(\gamma_{tc}+1)}{(\gamma_{tc}-1)}}}}}_{calculated\ thrust\ chamber\ pressure\ at\ i+1} \tag{4.5}$$

The (4.6), (4.7) and (4.8) of the equations in the set derive the gas-generator combustion-chamber pressure. Starting from the oxidizer-pump outlet, the oxidizer flow to the gas-generator combustion chamber passes in sequence through the gas-generator oxidizer line and its components (orifices, control valve, shutoff valve) and the oxidizer injector. The pressure loss generated across these hydraulic resistances must equal the difference between the oxidizer-pump discharge pressure and the gas-generator combustion-chamber pressure.

$$R_6 = \underbrace{P_{gg}}_{GG\ pressure\ at\ i} - \underbrace{(\underbrace{P_{tpe,o}}_{pump\ outlet\ pressure} - \underbrace{\sum_i \Delta P_{components,i}}_{hydraulic\ pressure\ losses})}_{calculated\ GG\ pressure\ at\ i+1} \tag{4.6}$$

Starting from the fuel-pump outlet, the fuel flow to the gas-generator combustion chamber passes in sequence through the gas-generator fuel line and its components (orifice, control valve), the gas-generator cooling channel, and the gas-generator fuel injector. The pressure loss generated across these hydraulic resistances must equal the difference between the fuel-pump discharge pressure and the gas-generator combustion-chamber pressure.

$$R_6 = \underbrace{P_{gg}}_{GG\ pressure\ at\ i} - \underbrace{\Big(\underbrace{P_{tpe,f}}_{pump\ outlet\ pressure} - \underbrace{\sum_i \Delta P_{components,i} \Big)}_{hydraulic\ pressure\ losses}}_{calculated\ GG\ pressure\ at\ i+1} \tag{4.7}$$

The Equation (4.8) uses the fuel and oxidizer mass flow rates supplied to the gas generator and derives the gas-generator combustion-chamber pressure. For determining the burned-gas properties, because the gas generator operates fuel-rich, obtaining a solution with CEA does not yield accurate results. Gas properties from Huzel's study were used.

$$R_8 = \underbrace{P_{gg}}_{GG\ Pressure\ at\ i} - \underbrace{\frac{(\dot{m}_o + \dot{m}_f)}{A_{n,gg}\sqrt{\dfrac{\gamma_{gg}}{R_{gg}T_{gg}}\left(\dfrac{2}{\gamma_{gg}+1}\right)^{\frac{(\gamma_{gg}+1)}{(\gamma_{gg}-1)}}}}}_{calculated\ GG\ pressure\ at\ i+1} \tag{4.8}$$

The velocity obtained from the isentropic expansion between the turbine nozzle inlet pressure and outlet pressure is determined by the relation given in the Equation (4.9). The parameter used to calculate the turbine power depends on the gas properties produced in the gas generator and on the pressure ratio across the turbine.

$$R_9 = \underbrace{C_{ad,tb}}_{Turbine\ adiabatic\ Velocity\ at\ i} - \underbrace{\sqrt{\frac{2\gamma_{gg}}{\gamma_{gg}-1} R_{gg}T_{gg}\left\{1-\left(\frac{P_{tbe}}{P_{gg}}\right)^{\frac{\gamma_{gg}-1}{\gamma_{gg}}}\right\}}}_{calculated\ Turbine\ Adiabatic\ Velocity\ at\ i+1} \tag{4.9}$$

Operation at different rotational speeds and pressure ratios affects turbine efficiency. Equation (4.10) in the set is used to calculate the turbine efficiency corresponding to these varying speeds and pressure ratios. The coefficients (A, B, C, D, E, F) belong to the correlation fitted to data over different speeds and pressure ratios. It is an empirical expression.

$$R_{10} = \underbrace{\eta_{tb}}_{turbine\ efficiency\ at\ i} - \underbrace{\begin{matrix}\left\{A_{tb}\left(\frac{P_{gg}}{P_{tbe}}\right)^2 + B_{tb}\left(\frac{P_{gg}}{P_{tbe}}\right) + C_{tb}\right\} x \left(\frac{D_{m,tb}n_{tp}}{2C_{ad,tb}}\right)^2 \\ + \left\{D_{tb}\left(\frac{P_{gg}}{P_{tbe}}\right)^2 + E_{tb}\left(\frac{P_{gg}}{P_{tbe}}\right) + F_{tb}\right\} x \left(\frac{D_{m,tb}n_{tp}}{2C_{ad,tb}}\right)\end{matrix}}_{calculated\ turbine\ efficiency\ at\ i+1} \tag{4.10}$$

For the pumps, the best-efficiency point mostly lies at the on-design condition. Equations (4.11) and (4.12) are the correlations used to represent pump efficiency at different rotational speeds and flow rates.

$$R_{11} = \underbrace{\eta_{tp,o}}_{oxidizer\ efficiency\ at\ i} - \underbrace{\left(a + b\dot{Q}_o + c{\dot{Q}_o}^2 + dn_{tp} + e{n_{tp}}^2 + f\dot{Q}_o n_{tp}\right)}_{calculated\ oxidizer\ pump\ efficiency\ at\ i+1} \tag{4.11}$$

$$R_{12} = \underbrace{\eta_{tp,f}}_{fuel\ pump\ efficiency\ at\ i} - \underbrace{\left(a + b\dot{Q}_f + c{\dot{Q}_f}^2 + dn_{tp} + e{n_{tp}}^2 + f\dot{Q}_f n_{tp}\right)}_{calculated\ fuel\ pump\ efficiency\ at\ i+1} \tag{4.12}$$

In this model, Equation (4.13) enforces the balance between the power produced by the turbine and the power consumed by the pumps. Using the calculated efficiency values for the turbine and the pumps, the equation is solved under the condition that the turbine's output power equals the pumps' power demand.

$$R_{13} = \underbrace{\frac{\eta_{tb} * {C_{ad,tb}}^2 \left(\dot{m}_{gg_o} + \dot{m}_{gg_f}\right)}{2}}_{Turbine\ Power} - \underbrace{\frac{\left(P_{tpi,o} - P_{tpi,o}\right) * \dot{Q}_o}{\eta_{tp_o}}}_{Oxidizer\ Pump\ Power} - \underbrace{\frac{\left(P_{tpe,f} - P_{tpi,f}\right) * \dot{Q}_f}{\eta_{tp_f}}}_{Fuel\ Pump\ Power} \tag{4.13}$$

For the solution to exist at a unique point, three additional equations that close the cycle are solved in the model.

Equation (4.14) calculates the turbine efficiency using the turbine inlet and outlet temperatures and the pressure ratio.

$$R_{14} = \underbrace{\eta_{tb}}_{turbine\ efficiency} - \underbrace{\frac{\left(T_{gg} - T_{0,tbe}\right)}{T_{gg}\left\{1 - \left(\frac{P_{tbe}}{P_{gg}}\right)^{\frac{\gamma_{gg}-1}{\gamma_{gg}}}\right\}}}_{calculated\ isentropic\ turbine\ efficiency} \tag{4.14}$$

Equation (4.15) calculates the Mach number at the turbine-nozzle exit using the turbine nozzle area ratio and the gas properties from the gas generator.

$$R_{15} = \underbrace{Ma_{tbe}}_{exit\ Mach\ at\ i} - \underbrace{\left(\frac{\gamma_{gg}+1}{2}^{-\frac{\gamma_{gg}+1}{2(\gamma_{gg}-1)}} \frac{\left(1+\frac{\gamma_{gg}-1}{2} Ma_{tbe}{}^{2}\right)^{\frac{\gamma_{gg}+1}{2(\gamma_{gg}-1)}}}{A_{tbe}/A^{*}} \right)}_{calculate\ nozzle\ exit\ mach\ number\ at\ i+1} \quad (4.15)$$

Finally, the turbine exit pressure is calculated based on the gas generator pressure, the turbine nozzle exit mach number, and the specific-heat ratio γ of the combustion products in the gas generator in the Equation (4.16).

$$R_{16} = P_{tbe} - (P_{gg} * (1 + \frac{\gamma_{gg}-1}{2} Ma_{tbe}{}^{2})^{\frac{-\gamma_{gg}}{\gamma_{gg}-1}}) \quad (4.16)$$

5. MODELLING & RESULTS

5.1 KRE-075

In order to demonstrate the static performance tool, Nuri (KSLV-II) is selected as the representative system, with the first-stage KRE-075 (sea-level) engine providing the baseline for model inputs and outputs. Figure 5.1 presents the design of the KRE-075 engine. The Nuri is a three-stage launch vehicle: the first stage is powered by four 75-tonf sea-level engines, the second stage by a single 75-tonf vacuum engine and the third stage by a 7-tonf engine [29]. While the development of small satellite launch vehicles (SLVs) focuses on acquiring launch vehicle system technologies, including launch vehicle system integration and launch operation technology, the development of the Korean launch vehicle (KLV) places the greatest emphasis on the development of high-thrust liquid propulsion engines, a technology that was relatively lacking in previous projects. Therefore, the successful development of a 75-ton liquid rocket engine is a key factor in determining the success or failure of the KLV development project. The 75-ton liquid engine for the KLV is based on the experience gained from the development of a 30-tonf liquid rocket engine by the Korea Aerospace Research Institute (KARI) as a preliminary research project on liquid engine technology during the development of the small satellite launch vehicle [30, 31].

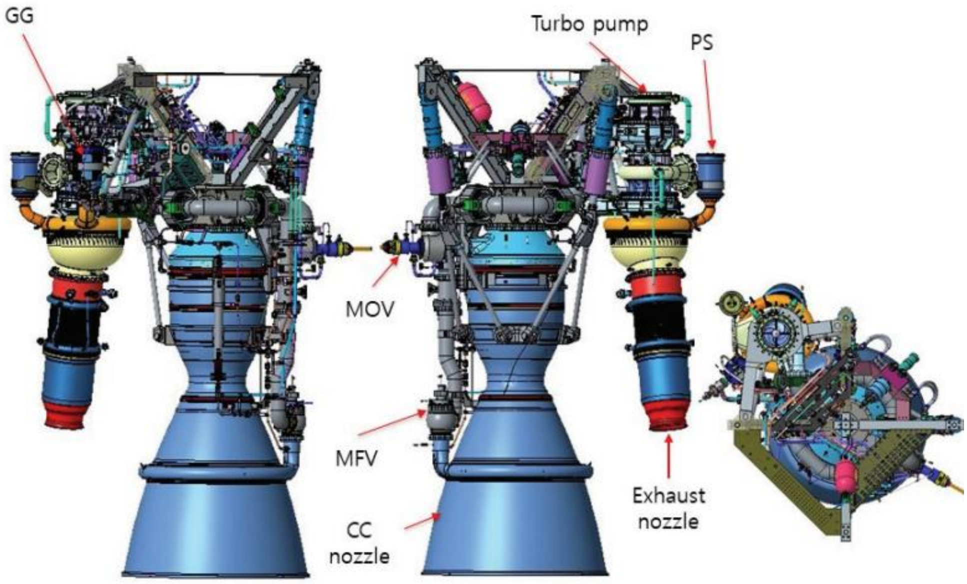

Figure 5.1: KSLV-II 75-tonf LRE [32]

A detailed P&ID of the KRE-075 from the literature was presented previously in Figure 2.8. Pre-ignition operations such as purge and chilldown belong to the transient phase that enables the engine start. Therefore, detailed P&ID includes pneumatic actutation system, chilldown and purge lines. A simplified P&ID is given in Figure 5.2 and this is adequate for steady and on-design performance analysis. This schematic includes on the turbopump, gas generator, thrust chamber and the hydraulic feed system (piping, valves and orifices).

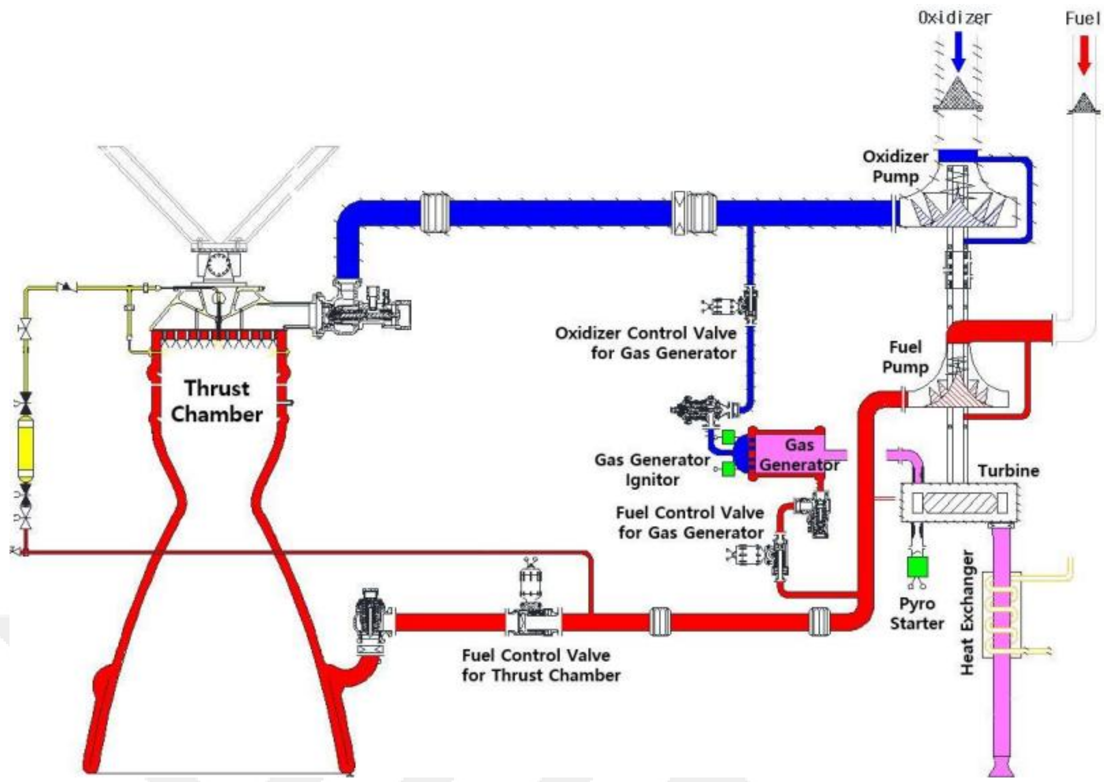

Figure 5.2: KRE – 075 Schematic [33]

In the KRE-075, the thrust chamber was designed for a combustion pressure of 60 bar and a mixture ratio (O/F) of 2.5. As indicated in Figure 5.3, under a shifting-chemical-equilibrium model the nozzle expansion ratio that maximizes vacuum specific impulse depends on mixture ratio. Therefore, the optimum expansion ratio differs across O/F values. Increasing oxidizer - fuel ratio raises the combustion-gas temperature and increases cooling requirements. Also, approximately 10% of the fuel flow is used to film cooling which causes higher O/F at center of combustion chamber. Therefore, the mixture ratio yielding the maximum vacuum specific impulse shifts to a lower value. Considering these factors, an O/F of 2.5 was selected [34].

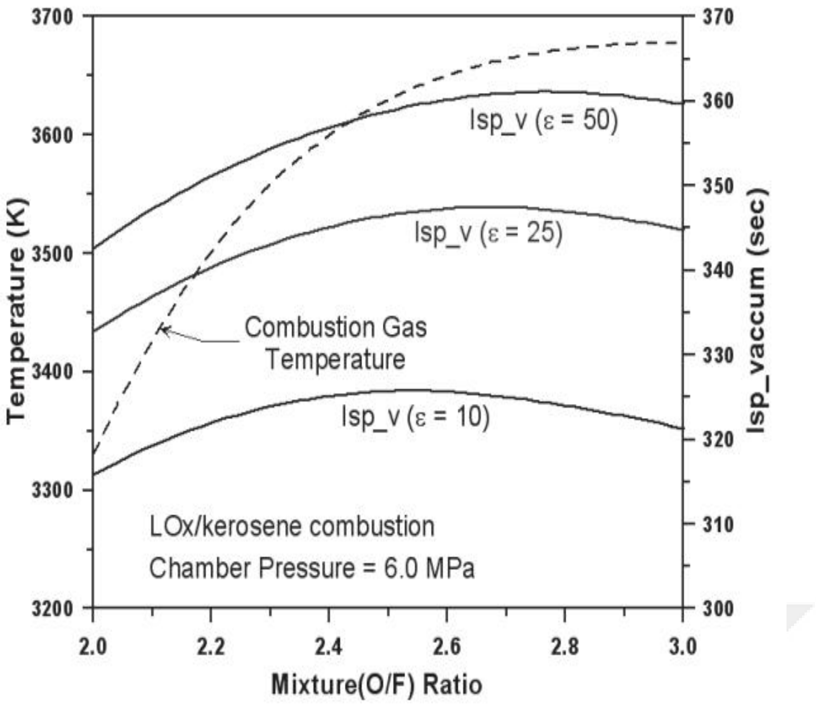

Figure 5.3: Combustion Temperature and Specific Impulse vs. Mixture Ratio [34]

The 75-tonf first-stage thrust chamber consists of a mixing head, a combustion chamber, and a nozzle. The chamber and nozzle have a double-wall construction which include an inner rectangular channel liner for regenerative cooling and an outer jacket that provides structural support. The temperature in combustion chamber and nozzle throat is high, therefore, a film cooling is placed at the entrance of combustion chamber and nozzle throat. Figure 5.4 shows 75-tonf thrust chamber desgin specifications.

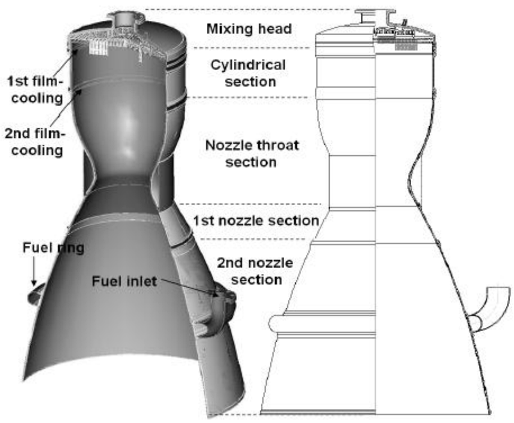

Chamber pressure		6.0 MPa
Mixture(O/F) ratio		2.45
Ignition method		TEA+TEB mixture
Propellant mass flow rate	Oxidizer	173.0 kg/s
	Fuel	70.6 kg/s
Characteristic velocity(C*)		1,730 m/s
Chamber diameter		524 mm
Throat diameter		302.5 mm
Nozzle exit diameter		1,048 mm
Nozzle expansion ratio		12.0
Thrust	Vacuum	74.8 tonf
	sea level	65.9 tonf
Specific impulse	Vacuum	306.9 sec
	sea level	270.6 sec

Figure 5.4: Thrust Chamber Design Specifications [34]

Figure 5.5 shows that the oxidizer and fuel injector manifolds deliver propellants to injectors with separate flow paths. Oxidizer enters via a central supply line and fills a dome-shaped oxidizer manifold. Then, oxidizer is delivered through the injectors into the chamber. Fuel is introduced at the secondary-nozzle section, routed through the cooling channels to cool the chamber and nozzle, and subsequently collected in the fuel manifold before injection. As shown in Figure 5.5, the head incorporates 721 injectors arranged in 15 concentric rows. Ignition reliability is enhanced by one central ignition swirl injector and six jet-type ignition injectors, each positioned in one of the six outer compartments formed by the baffle injector.

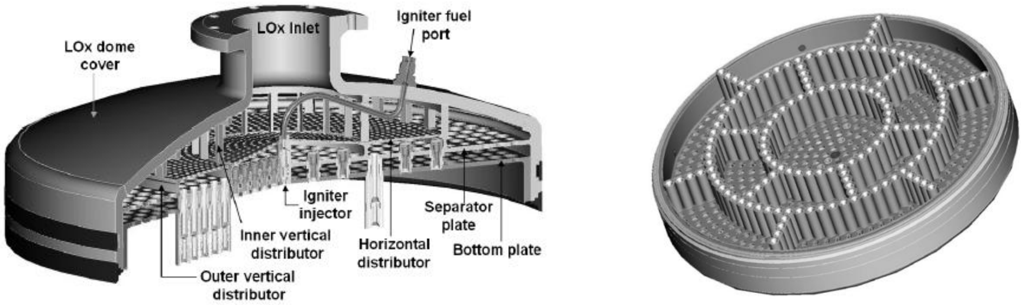

Figure 5.5: Mixing head and injector arrangements [34]

During thrust-chamber development, many experiments were performed, from scaled to full-scale combustors. The scaled 30-tonf engine tests show injector pressure drops of 11.5 bar for oxidizer and 14.0 bar for fuel at a chamber pressure of 60 bar with flow rates of 25.8 kg/s (fuel) and 63.0 kg/s (oxidizer) [35]. Figure 5.6 shows the 30-tonf combustor design and Figure 5.7 shows the 30-tonf engine test results.

Figure 5.6: 30-tonf Combustor [35]

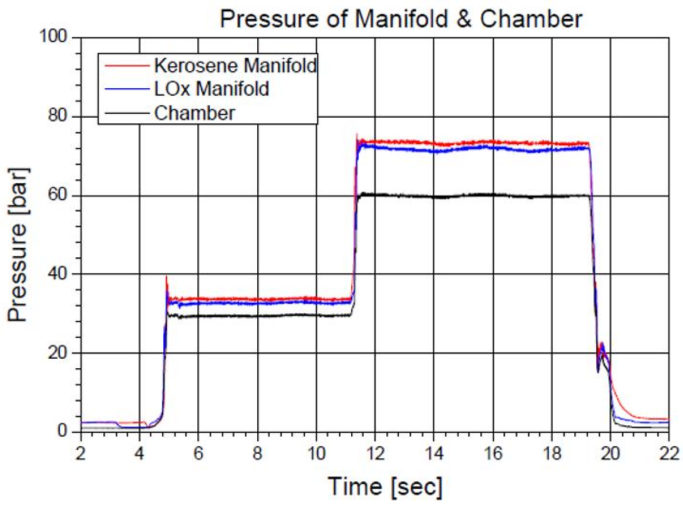

Figure 5.7: 30-tonf Engine Test Results [35]

In the scaled-engine tests, 277 injectors were used, whereas the full-scale 75-tonf engine has 721 injectors. Full scale development tests at 30 bar chamber pressure with a total flow rate of 121 kg/s show that injector discharge coefficients were similar to those from the scaled tests. These injector discharge coefficient data are used in the static model. Figure 5.8 shows the combustion chamber injector head that is used in the 75-tonf engine. Figure 5.9 shows the low pressure combustion test results of 75-tonf thrust chamber.

Figure 5.8: 75-tonf Combustion Chamber Injector Head [36]

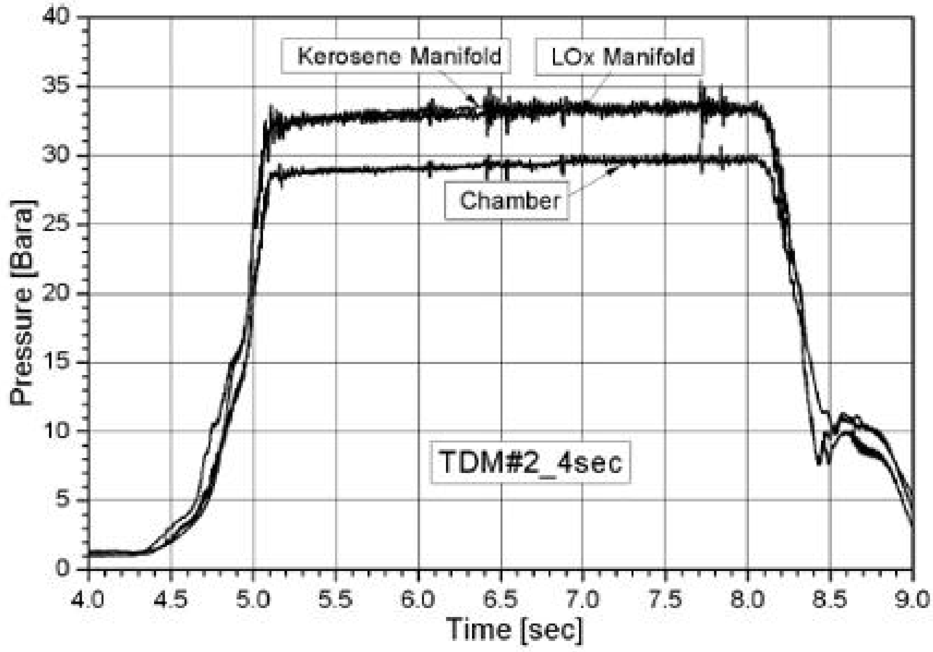

Figure 5.9: Low Pressure Combustion Test of 75-tonf Thrust Chamber [37]

The differential pressure generated in the regenerative cooling path generally has the largest portion of the thrust chamber's pressure drop and the design point pressure drop has been reported as 21 bar based on hydraulic analysis [34].

The gas generator used in KRE-075 consumes about 4% of the engine's total propellant flow rate to drive the turbine. The 75-ton-class gas generator (75tGG) is almost identical to the gas generator which was developed for 30-Tonf LOX/Kerosene rocket engine. The specifications of this gas generator are given in Table 5.1.

Compared to the 30-tonf gas generator, the main difference in the 75-tonf gas generator is an approximately threefold increase in propellant flow rate, consistent with the higher thrust level. The 75-tonf class gas generator adopted a similar cylindrical combustion chamber design, coaxial swirl injectors, and regenerative cooling concept as the 30tGG, based on the previously developed technology [7]. Figure 5.10 shows the design of 30-tonf gas generator. The 75-tonf class gas generator specifications are given in Table 5.2.

Table 5.1: 30ton-f Gas Generator Requirements [31]

Operation Mode		Fuel-Rich	Unit
Propellant	Oxidizer	LOX	-
	Fuel	Jet A-1	-
Chamber Pressure		5.78	MPa
Gas Temperature		900	K
O/F Ratio		0.321	-
Mass Flow Rate	Fuel	3.33	kg/s
	Oxidizer	1.07	kg/s
	Total	4.40	kg/s
Residence Time		6.0	msec
Injector Pressure Drop	Fuel	1.2	MPa
	Oxidizer	1.2	MPa
Spatial Temperature Distribution		<±70	K
Chamber Pressure Fluctuation		<3%	-

Figure 5.10: 30-tonf LPRE Gas Generator [7]

Developed gas generator for KRE-075 has typically fuel rich gas generator and combustion gas temperature is limited because of turbine blade structural limits [21].

Table 5.2: KRE-075 Gas Generator Specifications [21]

Specification	Value	Unit
Chamber Pressure	6.05	MPa
Total Propellant Flow Rate	10.3	kg/s
Burnt Gas Temperature	900 ± 70	K
Weight	<11.2	kg

The KRE-075 turbopump consists of an oxidizer pump and a fuel pump driven by a turbine. Figure 5.11 shows the turbopump of the 75-tonf engine.

Figure 5.11: 75-tonf Turbopump Assembly [38]

Within the turbopump development effort for the 75-tonf engine, the specifications and design-point performance data collected from the literature are summarized in Table 5.3.

Table 5.3: Turbopump Design Requirements and Performance [38,39]

Components	Fluid	Flow Rate (kg/s)	Pressure (MPa)	Temperature (K)	N_s	ϕ	ψ	Specific Power (kJ/kg)	RPM
LOX Pump	Liquid Oxygen	175.6	8.4 + P_{in}	93	217	0.095	1.12		
Fuel Pump	Kerosene	79.3	11.0 + P_{in}	288	109	0.096	1.32	261	10300
Turbine	GG gas	11.3	5.8	900	-	-	-	-	

Pump development tests were performed based on similarity rules. Water tests of the fuel pump provided the data on flow ratio versus head coefficient and flow ratio versus efficiency at different rotational speeds [40]. Figure 5.12 and Figure 5.13 show the water test results for the fuel fump. The oxidizer pump tests were also conducted using water and results are presented as shown in Figure 5.14, Figure 5.15 and Figure 5.16 [41].

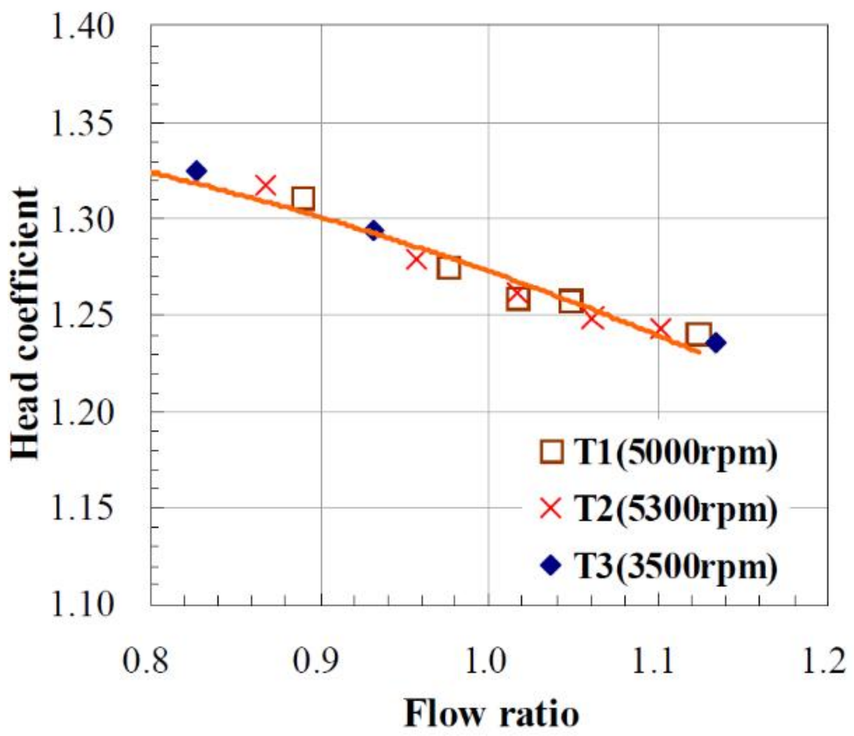

Figure 5.12: Head Coefficient versus Flow Ratio for the Fuel Pump [40]

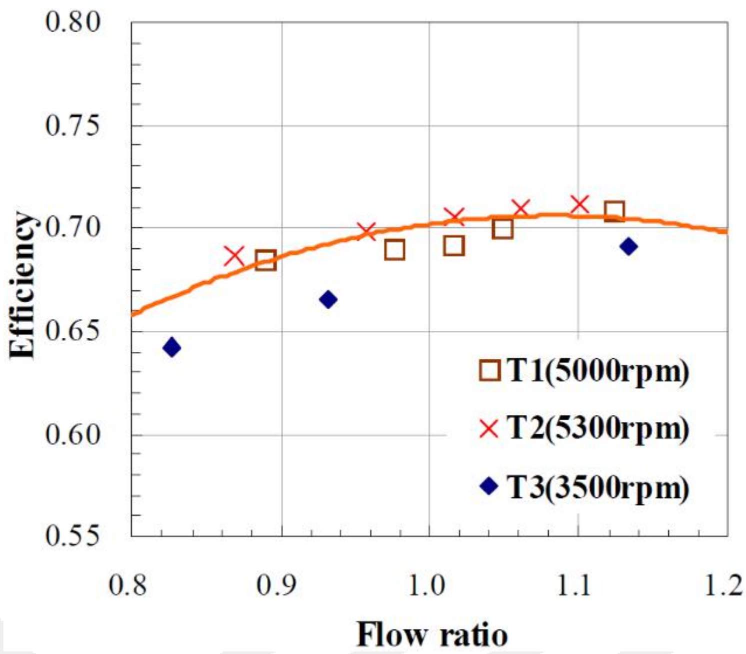

Figure 5.13: Efficiency versus Flow Ratio for the Fuel Pump [40]

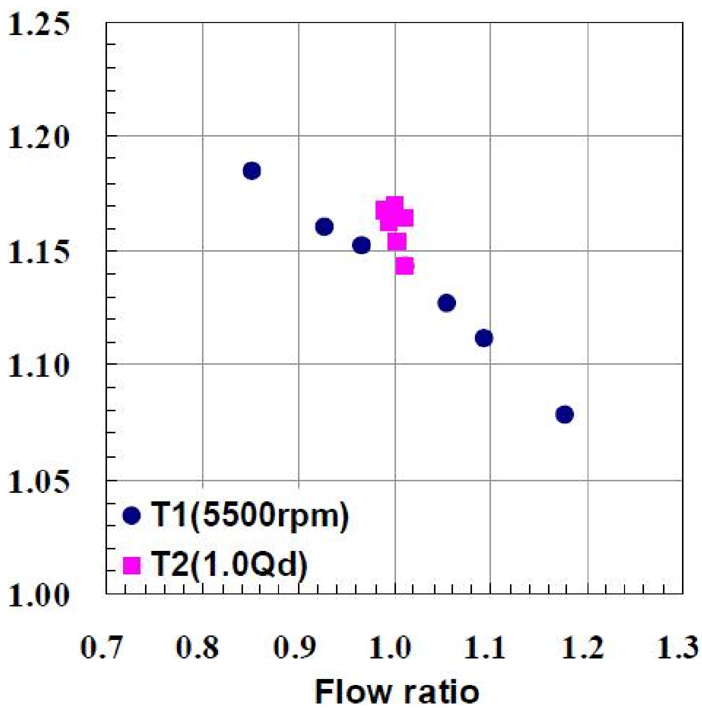

Figure 5.14: Head Coefficient versus Flow Ratio for the LOX Pump [41]

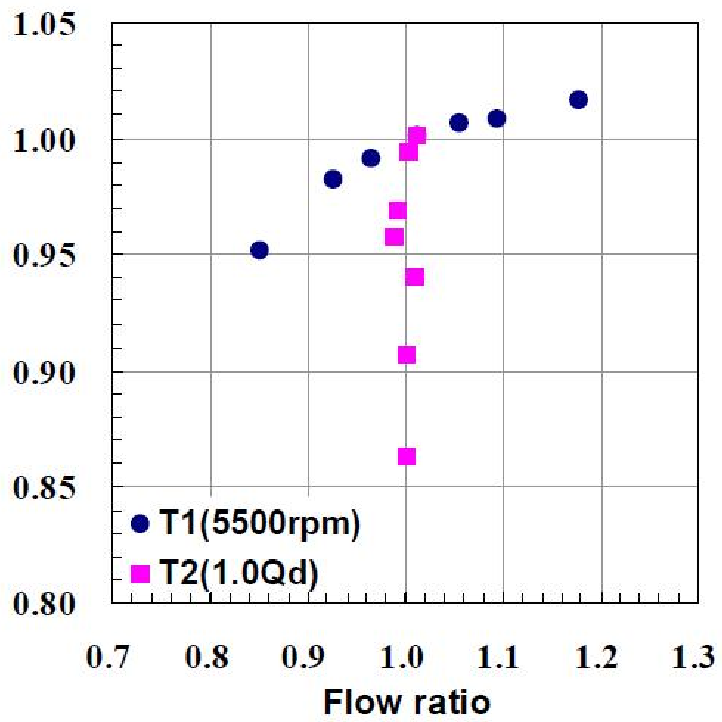

Figure 5.15: Efficiency versus Flow Ratio for the LOX Pump [41]

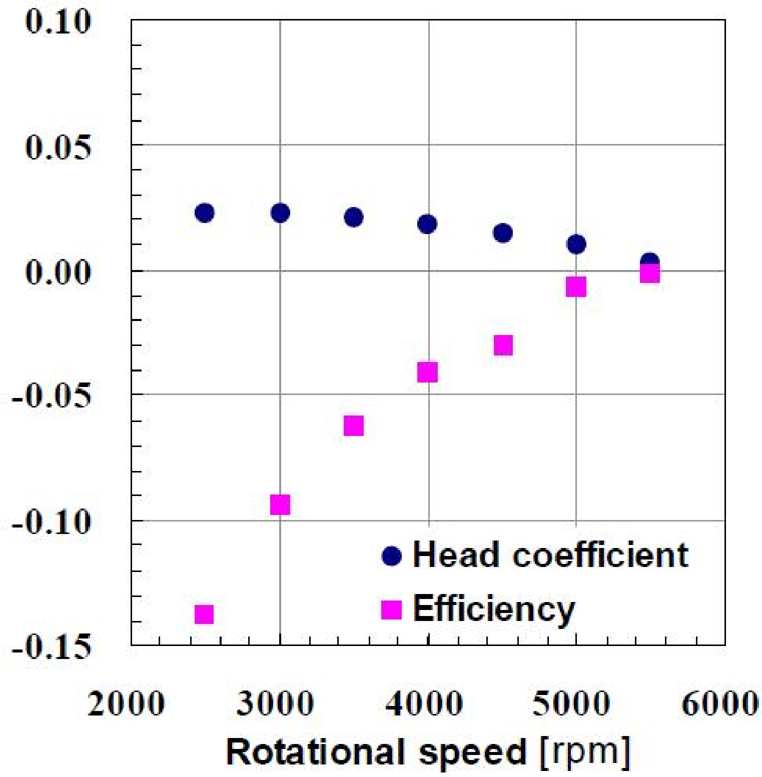

Figure 5.16: LOX Pump Head Coefficient and Efficiency at Different Speeds [41]

The turbine supplying power to the pumps comprises 12 nozzles, including 10 for steady operation and 2 for start-up. Figure 5.17 presents the turbine nozzle and rotor. Turbine specifications are provided in Table 5.4.

Figure 5.17: Turbine Nozzle and Rotor [42]

Table 5.4: 75tonf Turbine Specifications [42]

Parameter	Design Condition
Medium	GG Gas
Pressure Ratio	18
U/Cad	0.21
Nozzle No	10
Inlet Temperature [K]	900

The turbine was tested using air under similarity conditions to simulate the design point. The performance curves are derived using the corrected rotational speed (N*). Figure 5.18 shows the turbine efficiency for different pressure ratios and tip speed to adiabatic velocity ratios.

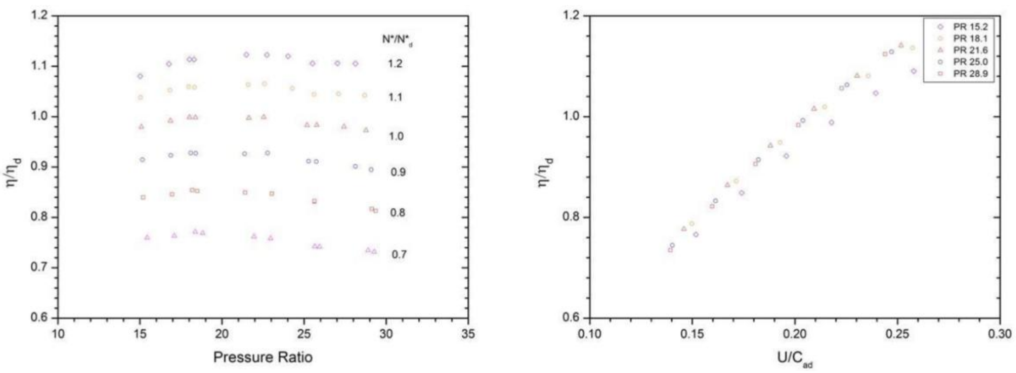

Figure 5.18: Turbine Efficiency versus Pressure Ratio and U/Cad [42]

In KRE-075, 4 shut off valves were used. Two of them are thrust chamber oxidizer and fuel valves, the other two are oxidizer and fuel valves for gas generator. These valves are poppet type and pneumatically actuated. Flow coefficients were derived from CFD analyses and water tests. Figure 5.19, Figure 5.20 and Figure 5.21 show the main oxidizer valve, the thrust chamber fuel valve and the gas generator fuel valve along with their test results, respectively.

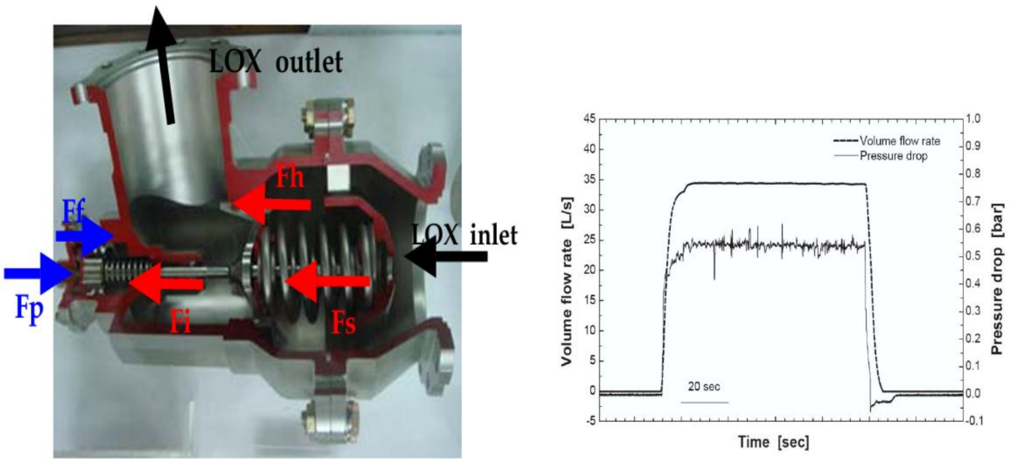

Figure 5.19: Main Oxidizer Valve and Water Test Result [43,44]

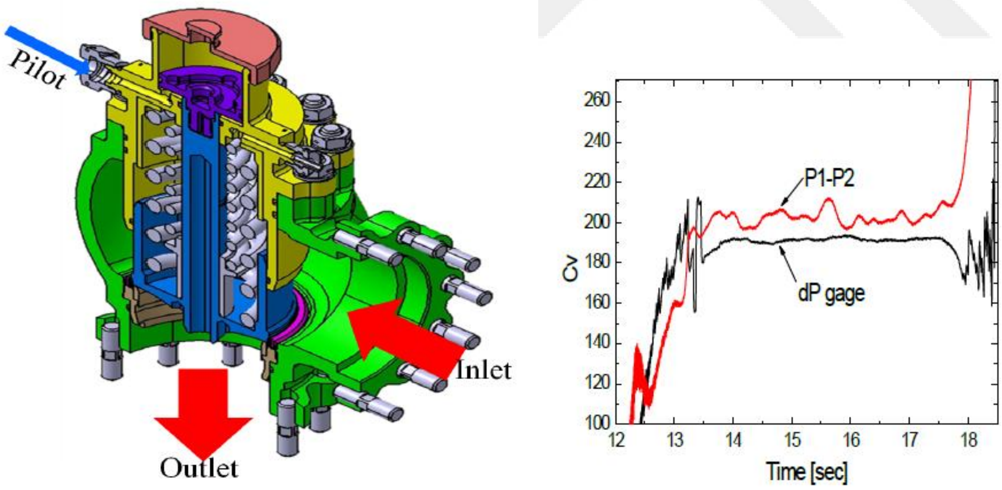

Figure 5.20: Thrust Chamber Fuel Valve Design and Valve Coefficient Test [45]

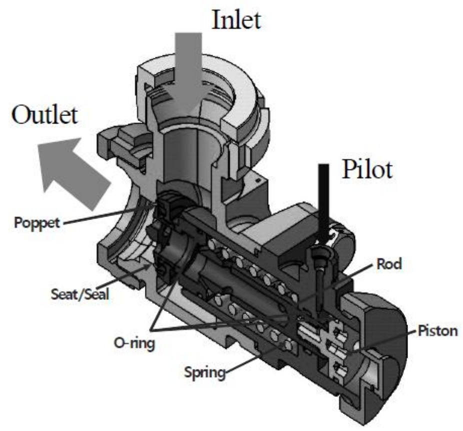

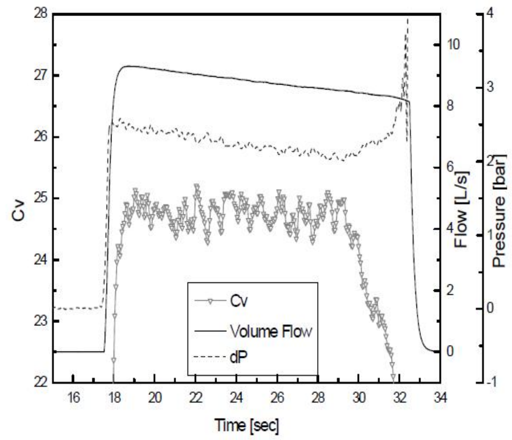

Figure 5.21: Gas Generator Fuel Valve and Test Result [46]

The KRE-075 engine has also control valves used to regulate flow. By setting these valves to different positions, pressure drops can be changed and the flow rate can be adjusted. Three control valves are used in the engine. These valves are located as follows: one in the gas-generator oxidizer line, one in the gas-generator fuel line, and one in the thrust-chamber fuel line. The Kv characteristics of the gas generator control valves are shown in Figure 5.22.

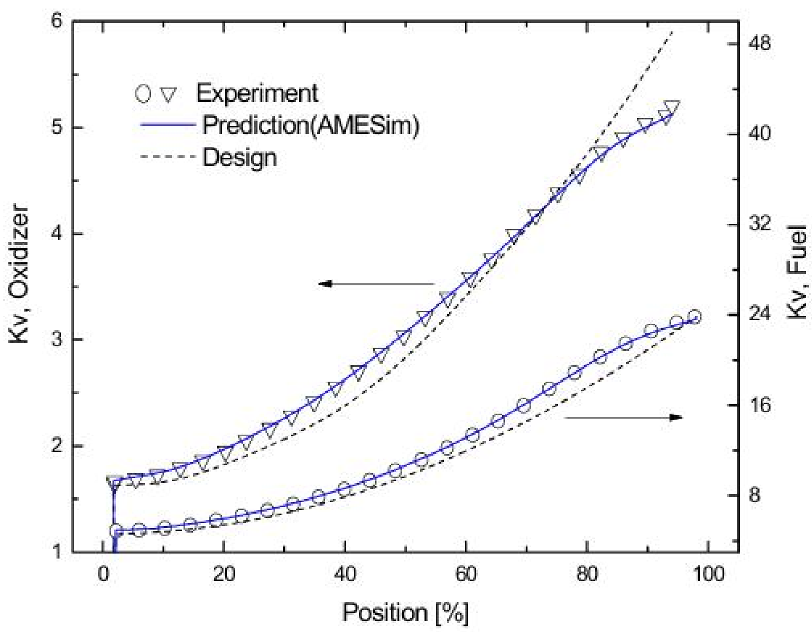

Figure 5.22: Kv Values of the Fuel and Oxidizer Control Valves [47]

5.2 Results

Results were obtained for the gas-generator control valves and the thrust chamber control valve positions using the developed model. For the assumed nominal valve positions, Table 5.5 summarizes the specification/requirement targets for the turbopump, gas generator and thrust chamber with difference model predicted values. In addition, three parametric cases evaluated to quantify how changes in each control valve position affect overall system performance.

Table 5.5 also provides a comparison between the model predictions and the specifications for the relevant component performance parameters. Under the assumptions given in 5.1 KRE-075, the largest deviation occurs in the gas generator mass flow rate. Because the gas generator produced gas properties were taken from Huzel's tabulations, error in the predicted turbine power is expected. Therefore, the results can be judged acceptable. The model results that thrust slightly above the reference value but lower the specific impulse. Achieving a similar thrust with higher mass flow rate causes the lower specific impulse.

Treating these results as the nominal baseline, outcomes for the three control valve cases are presented next.

Table 5.5: Model Nominal Results

Parameter	Model Result	KRE-075	Difference (%)
Fuel Pump Flow Rate (kg/s)	79.58	79.3	0.35
Oxidizer Pump Flow Rate (kg/s)	176.5	175.6	0.51
Turbopump RPM	10365	10300	0.63
LOX Pump	85.1025 + Pin	84+ Pin	1.31
Fuel Pump	116.31 + Pin	110+Pin	5.74
GG O/F	0.3217	0.321	0.22
GG Total Flow Rate (kg/s)	10.75	10.3	4.37
GG Pressure	63.41973	60.5	4.83
Turbine Inlet Temperature (K)	897	900	0.33
Turbine PR	19.31	18	7.28
TC LOX Flow Rate (kg/s)	173.8712	173.0	0.5
TC Fuel Flow Rate (kg/s)	71.44249	70.6	1.19

Table 5.6 (continued): Model Nominal Results

Parameter	Model Result	KRE-075	Difference (%)
TC O/F	2.434	2.45	0.65
TC Total Flow Rate (kg/s)	245.31	243.6	0.7
TC Pressure (bar)	59	60	1.67
TC Regenerative Cooling (bar)	21.69952	21	3.33
TC Sea Level Thrust (tonf)	66	65.9	0.15
TC Vacuum Level Thrust (tonf)	74.9	74.8	0.13
TC Vacuum Specific Impulse (s)	305.4	306.9	0.49

5.2.1 Gas generator oxidizer control valve throttling

Figure 5.23, Figure 5.24 and Figure 5.25 show how engine performance varies as the gas generator oxidizer control valve (OCV) opens. As the gas generator oxidizer control valve (OCV) opens, the oxidizer flow to the gas generator increases, raising the gas generator mixture ratio (O/F). The higher O/F elevates the gas temperature, which in turn increases turbine power and drives the turbopump to a higher speed. With higher turbine produced power, both oxidizer and fuel pump outlet pressures rise. Thus, total propellant flow rates drawn by engine increase. Consequently, not only the gas generator oxidizer flow but also the gas generator fuel flow increases, so the total gas generator mass flow rises. The increased pump discharge also raises the oxidizer and fuel flows to the thrust chamber, leading to a higher thrust level.

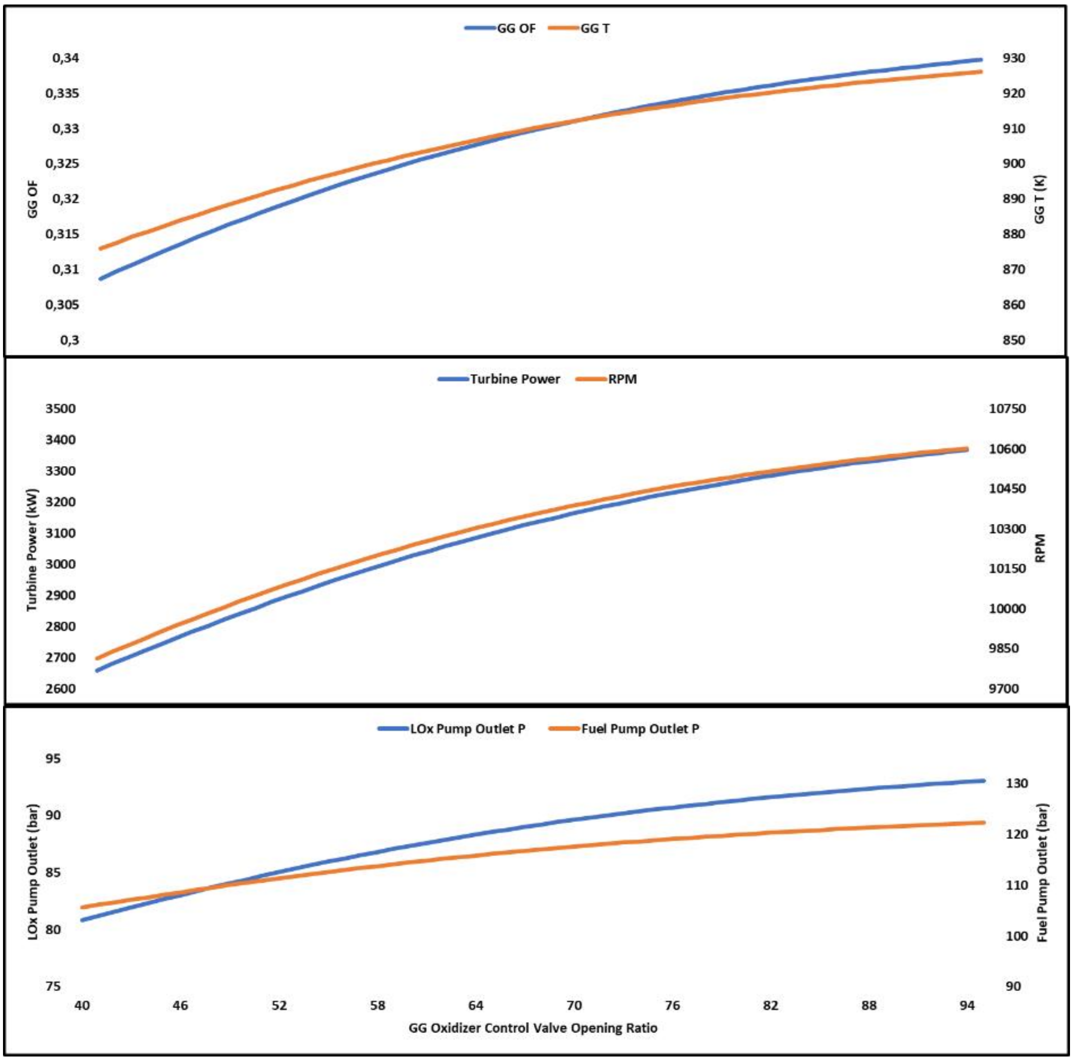

Figure 5.23: GG Mixture Ratio, Gas Temperature, Turbine Power, Turbopump RPM, Pump Outlet Pressures vs. GG OCV Position

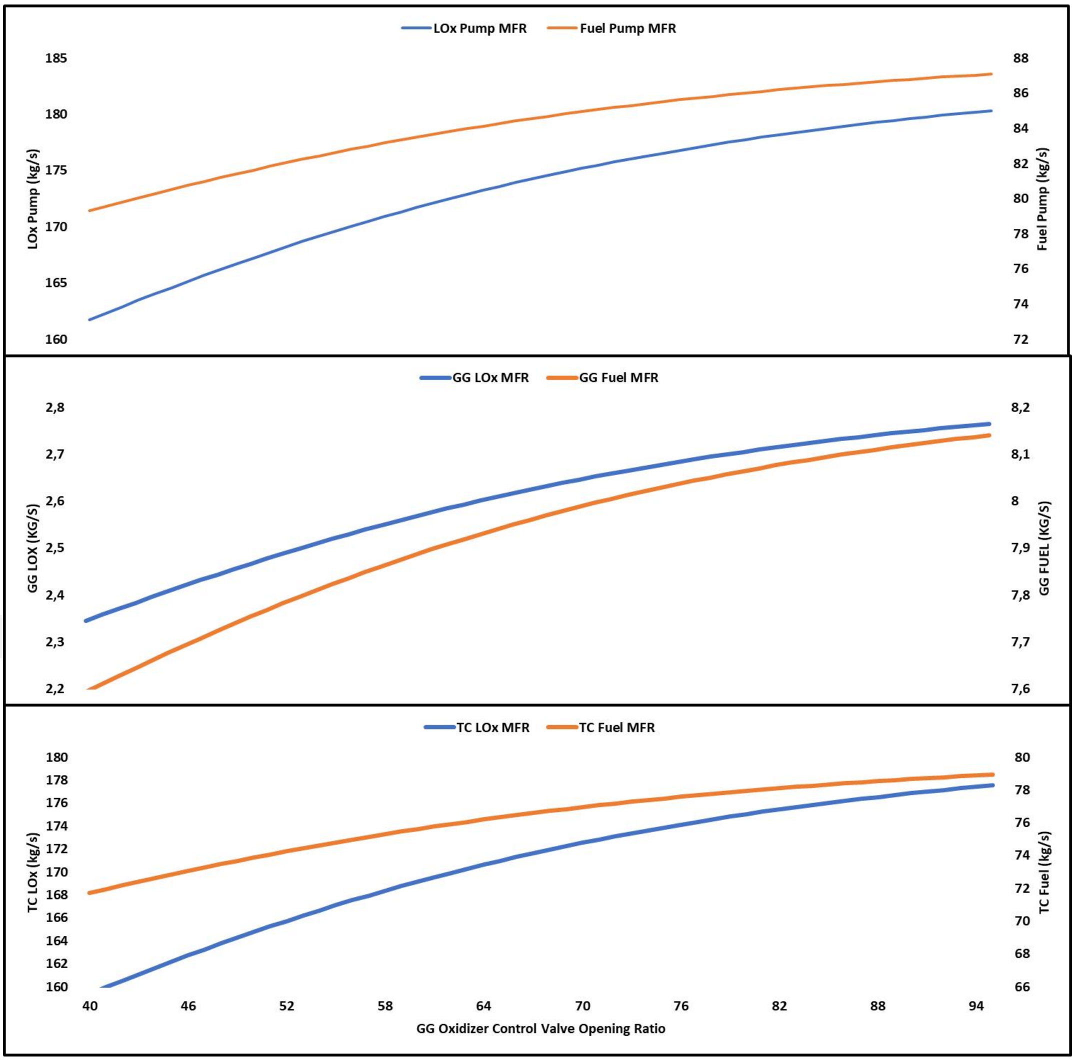

Figure 5.24: Pump Mass Flow Rates, GG Oxidizer and Fuel Flow Rates, TC Oxidizer and Fuel Flow rates vs. GG OCV Position

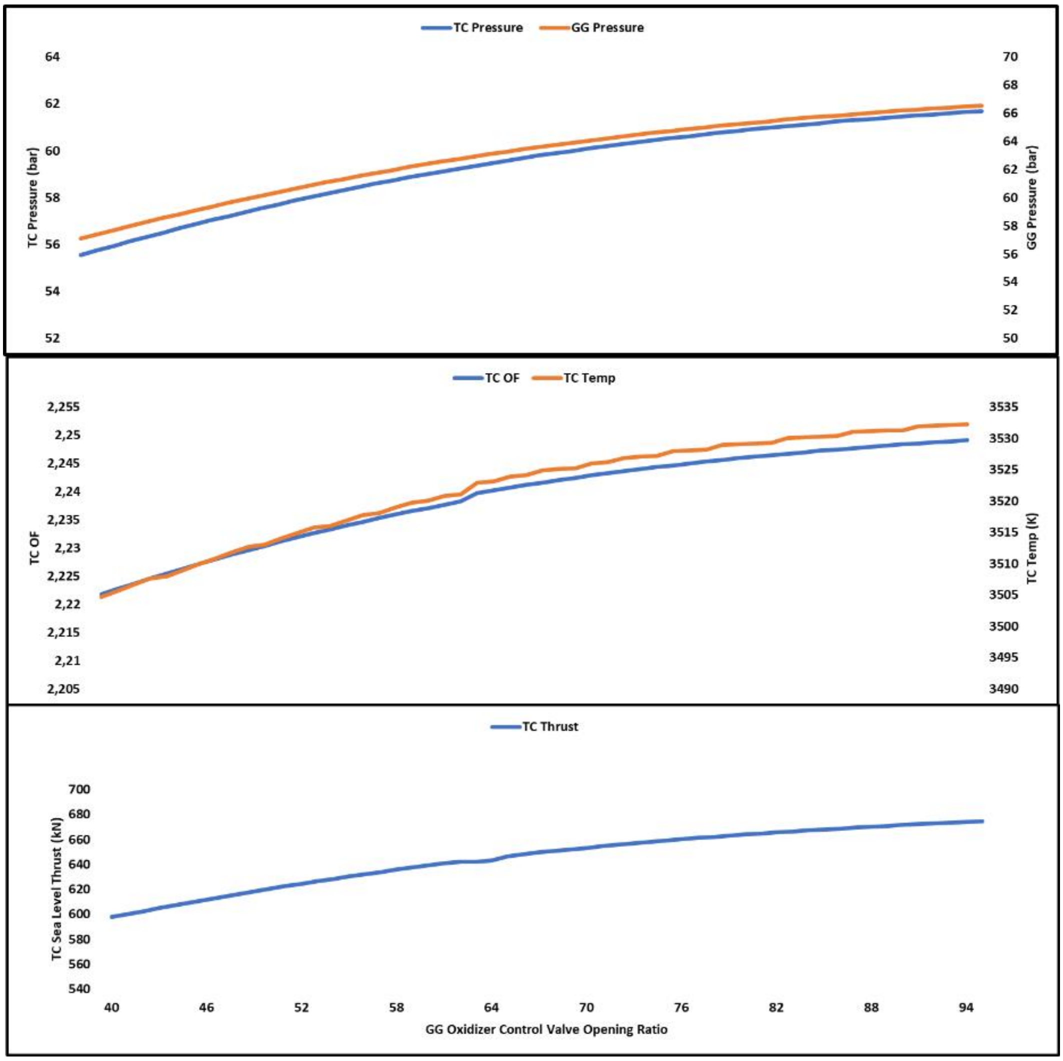

Figure 5.25: TC and GG Pressure, TC O/F, TC Gas Temperature, TC Thrust vs. GG OCV Position

5.2.2 Gas generator fuel control valve throttling

Figure 5.26, Figure 5.27 and Figure 5.28 demonstrate how engine performance responds to variations in the opening position of the gas generator fuel control valve. As the gas generator fuel control valve opens, the gas generator mixture ratio (O/F) decreases. The lower mixture ratio reduces the gas temperature at the gas generator and, in turn, turbine power. With less power available, pump outlet pressures decrease. Therefore, gas generator oxidizer flow decreases even though the gas generator fuel flow increases. Although the total gas generator mass flow rate rises, the dominant effect on turbine power is the reduction in mixture ratio. The reduced pump outlet pressures also reduce the propellant flows to the thrust chamber. Thus, thrust decreases due to the reduced thrust chamber flow rate.

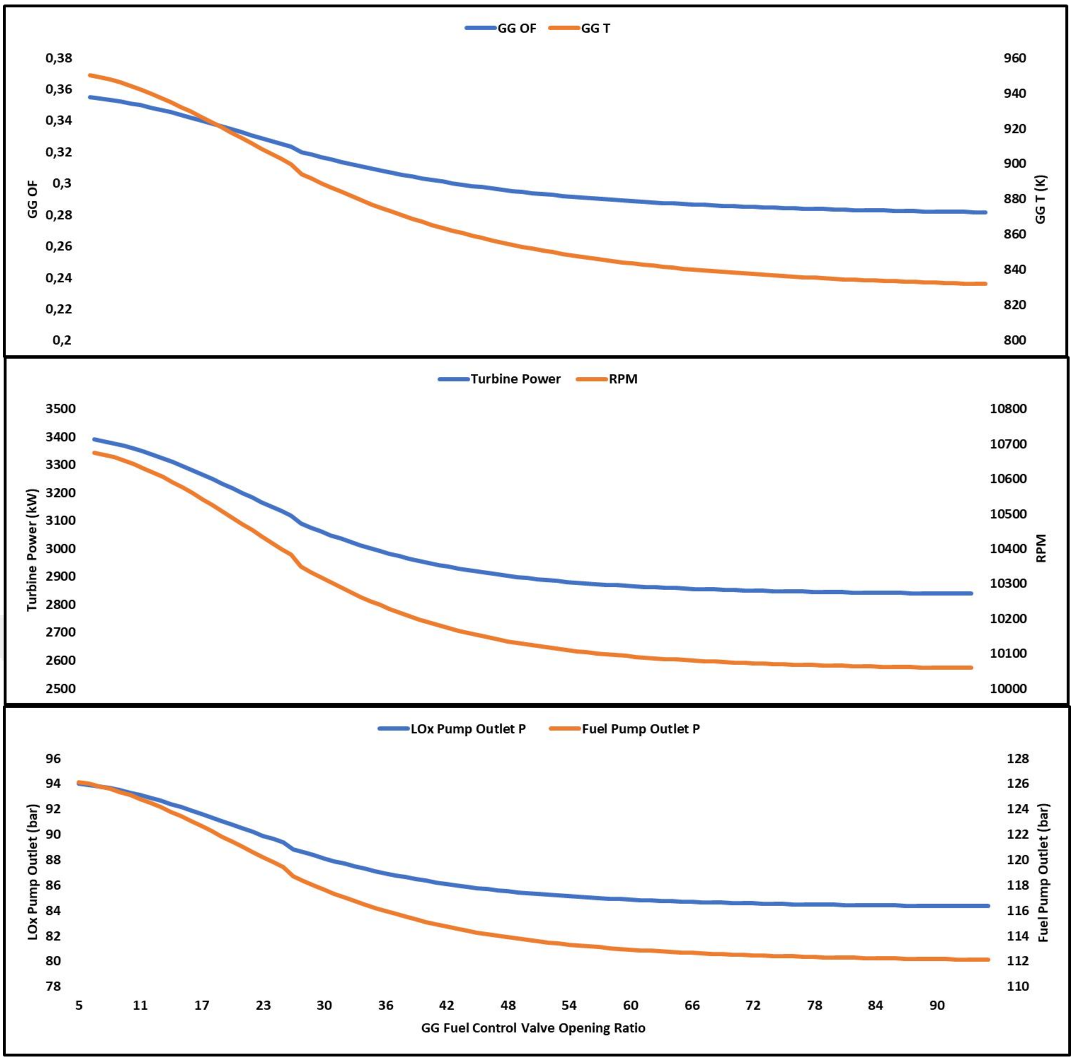

Figure 5.26: GG Mixture Ratio, Gas Temperature, Turbine Power, Turbopump RPM, Pump Outlet Pressures vs. GG FCV Position

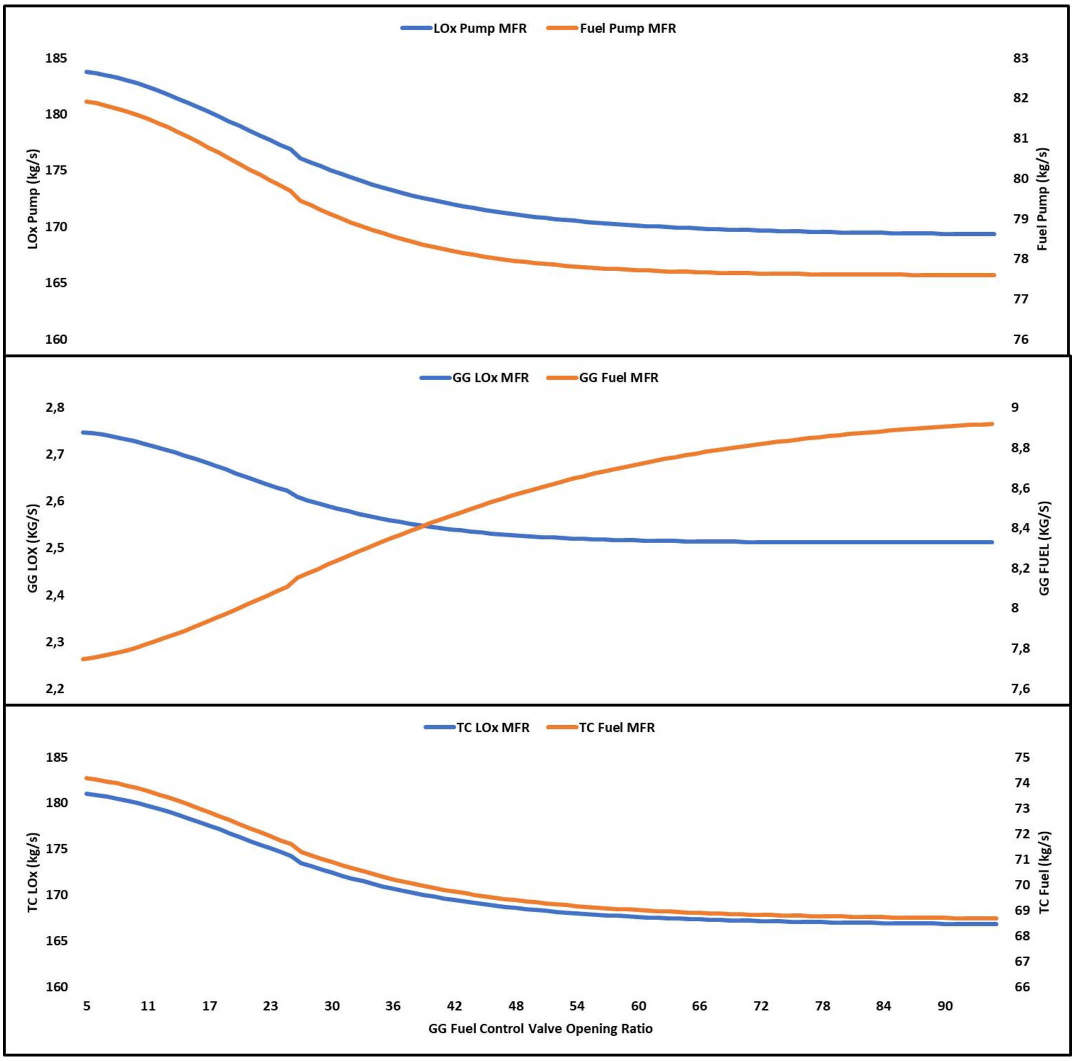

Figure 5.27: Pump Mass Flow Rates, GG Oxidizer and Fuel Flow Rates, TC Oxidizer and Fuel Flow rates vs. GG FCV Position

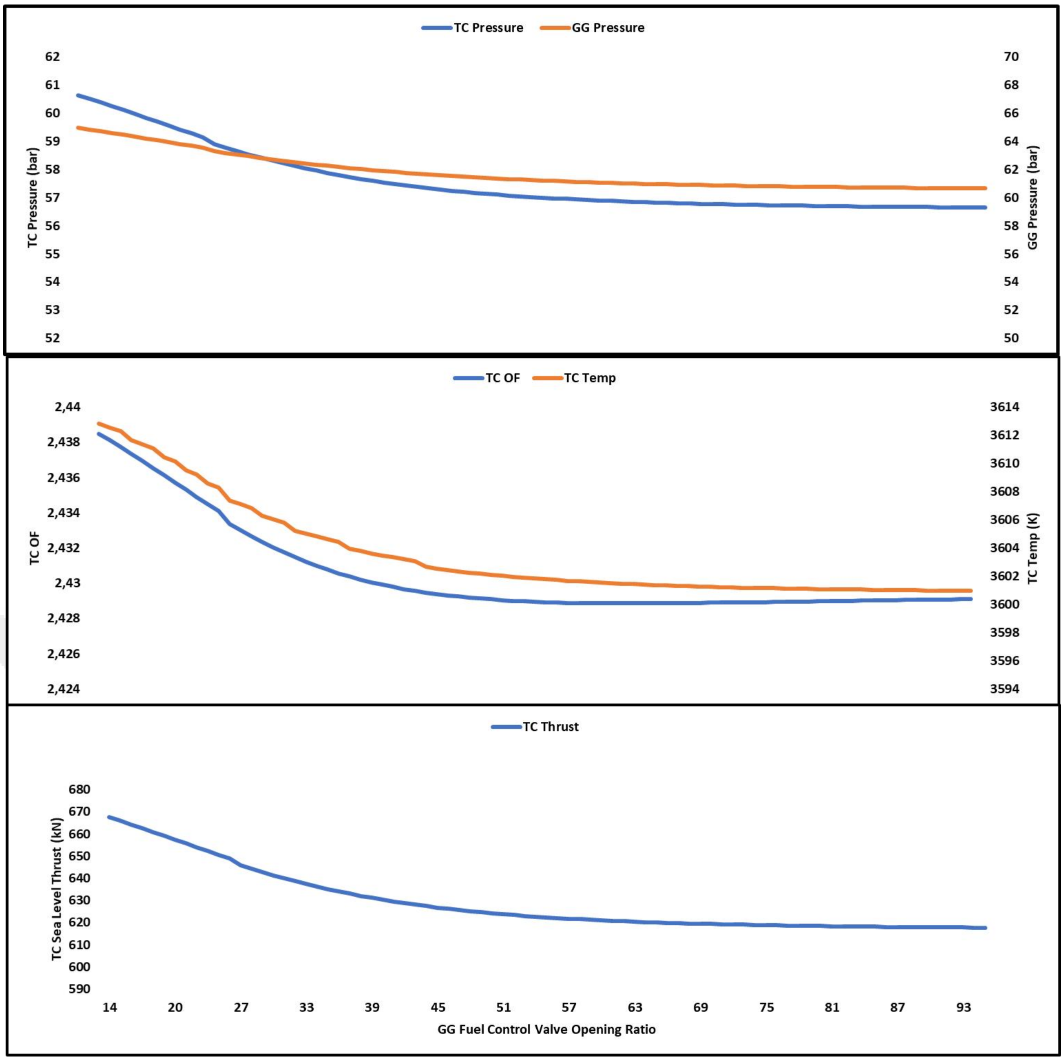

Figure 5.28: TC and GG Pressure, TC O/F, TC Gas Temperature, TC Thrust vs. GG FCV Position

5.2.3 Thrust chamber fuel control valve throttling

Figure 5.29, Figure 5.30 and Figure 5.31 illustrate the variation in engine performance as the thrust chamber fuel control valve opens. The LPRE performance results were generated for the thrust chamber fuel control valve that is the third control valve in the KRE-075 P&ID. Opening this valve reduces hydraulic resistance in the chamber fuel line, a greater share of the pump delivered fuel goes to the thrust chamber while the gas generator fuel flow decreases. This shifts the gas generator to a higher mixture ratio and raises the gas generator gas temperature. However, the reduction in total flow rate of gas generator causes the reduction turbine power. Decreasing turbine power leads to less pump outlet pressures. Fuel pump outlet pressures are more affected due to higher delivering fuel flow rate due to reduction resistance of chamber fuel line. As a result, oxidizer flows to both the gas generator and the thrust chamber decrease only marginally. Overall, the thrust chamber fuel control valve has a much smaller system level impact than the gas generator control valves. These are concluded that thrust chamber fuel control valve is better suited for trimming the chamber mixture ratio than for active thrust control.

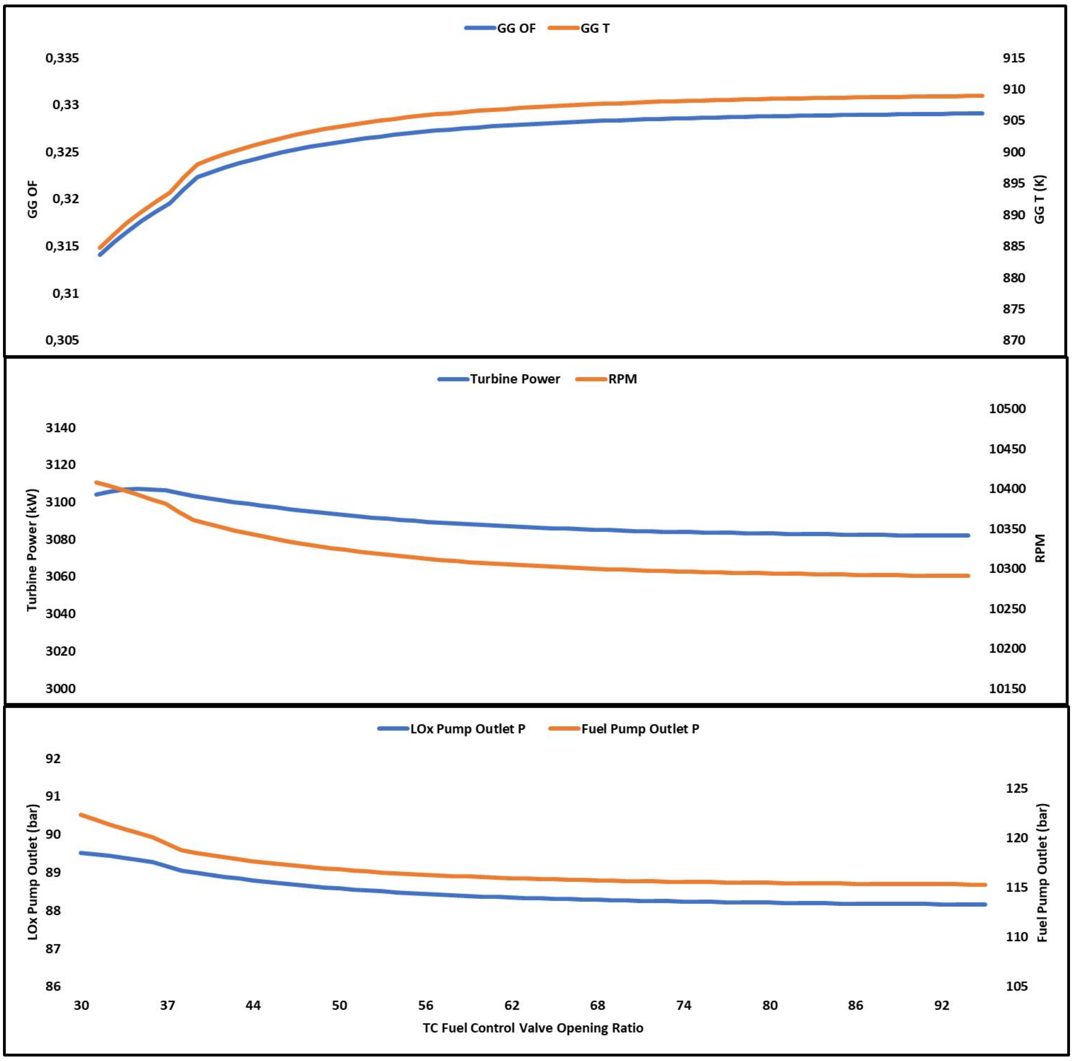

Figure 5.29: GG Mixture Ratio, Gas Temperature, Turbine Power, Turbopump RPM, Pump Outlet Pressures vs. TC FCV Position

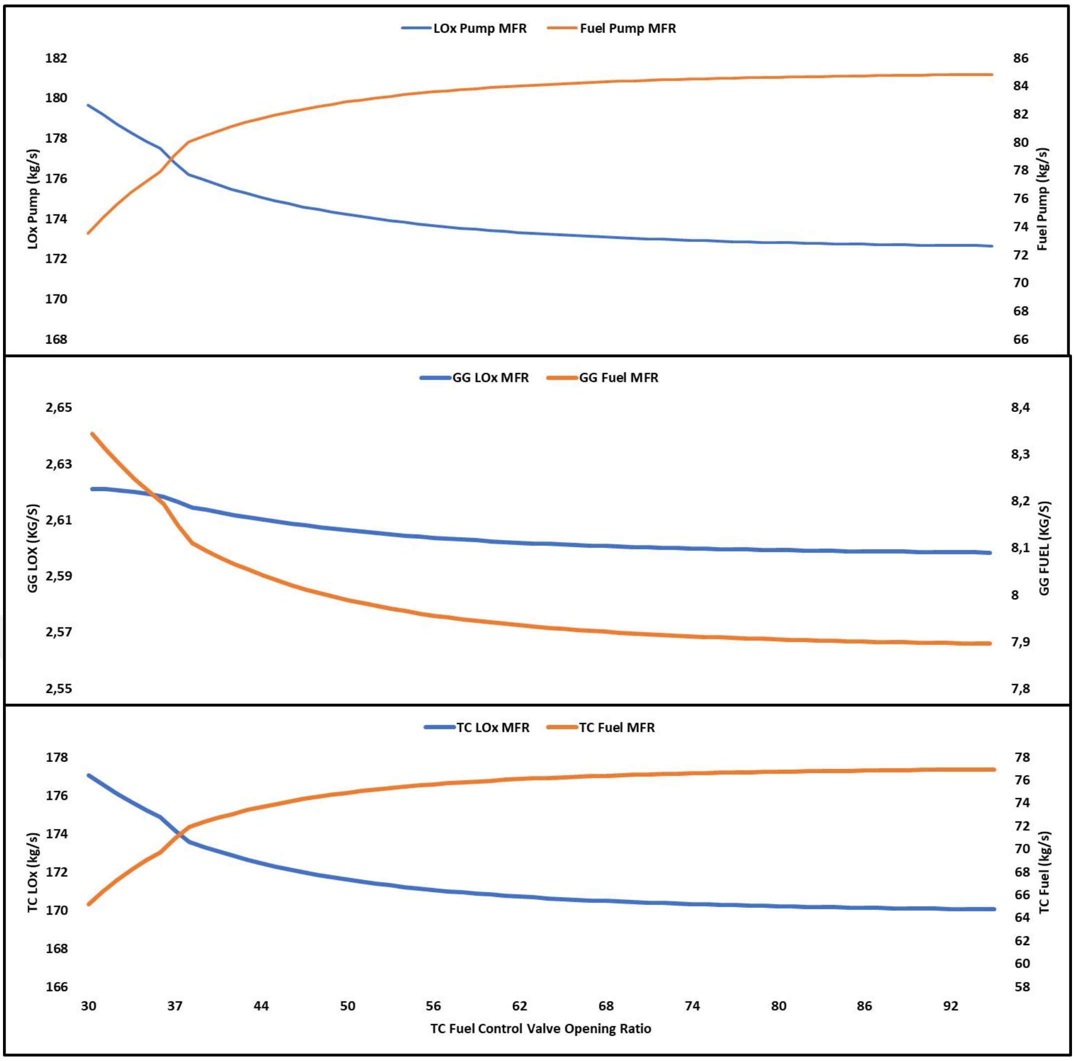

Figure 5.30: Pump Mass Flow Rates, GG Oxidizer and Fuel Flow Rates, TC Oxidizer and Fuel Flow rates vs. TC FCV Position

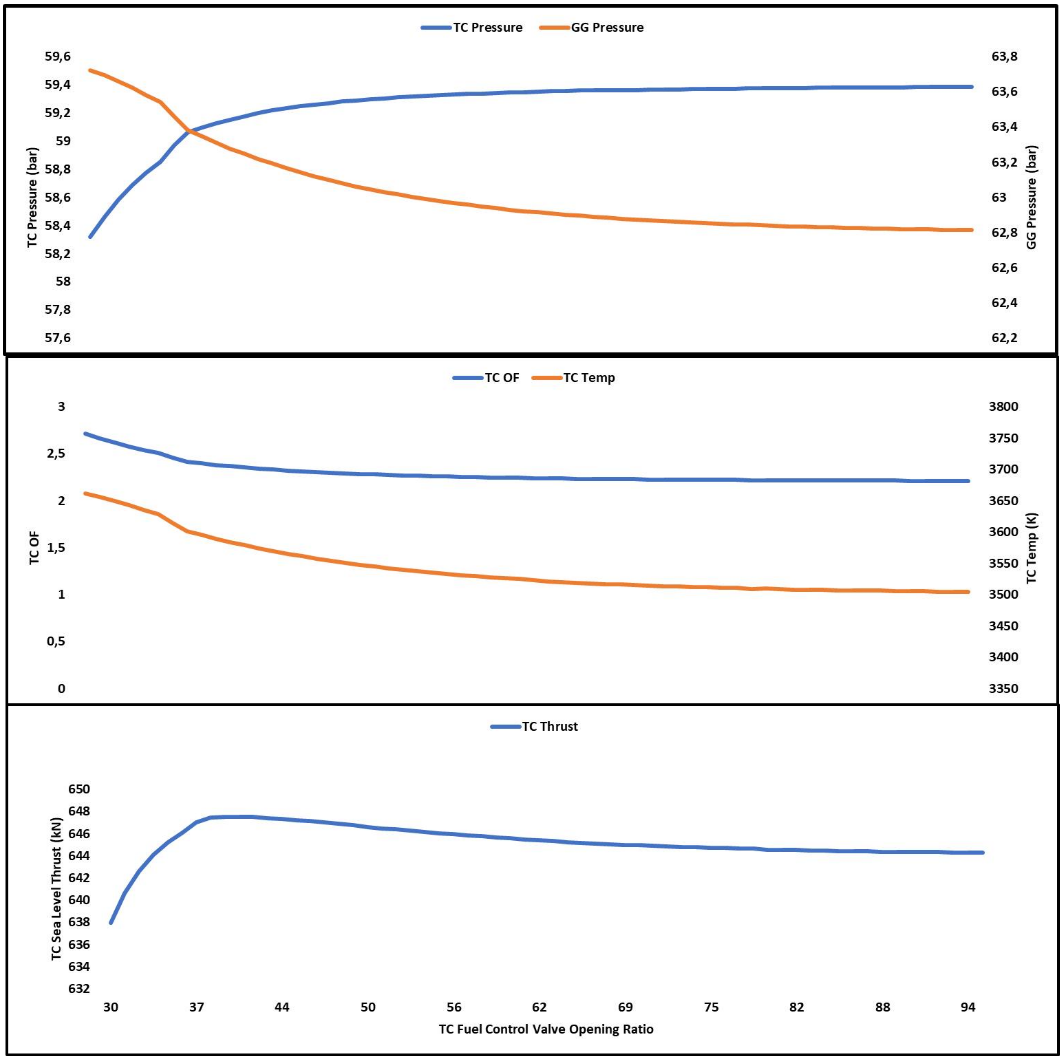

Figure 5.31: TC and GG Pressure, TC O/F, TC Gas Temperature, TC Thrust vs. TC FCV Position

6. CONCLUSIONS

In this thesis, a static performance model was developed for a gas generator (open cycle) liquid propellant rocket engine. The model resolves station level quantities (e.g., valve pressure drops, gas generator pressure, turbine power) and shows how changes in component level parameter affects to overall engine performance. While 1D transient simulations are typically preferred for dynamic analysis, the developed static model is less computationally expensive and therefore better suited to trade studies and early design decisions.

This static model calculates each engine station performance parameters (e.g., valve pressure drops, gas generator pressure, turbine power) and reveal effects of each performance parameters on overall engine performance. 1D dynamic models are mostly preferred to simulate engine performance but it has higher time compared to developed static model. In preliminary design phases, this model gives more fast response of development process and give you good idea when you have to take critical decision regarding to design of components.

For execution and comparison, the model was parameterized with publicly available KRE-075 data and its outputs were benchmarked against specification values. Because most of the source data originate from development testing, perfect agreement with flight hardware is not expected. Under the stated assumptions in 5.1 KRE-075, the discrepancies are judged acceptable. The large deviation appears in the gas generator mass flow rate (~5%) because the model uses Huzel's tabulated fuel rich product gas properties.

The primary aim of this study was to evaluate the off-design behavior of an LPRE. Varying control valve positions shows that throttling is governed primarily by the gas-generator oxidizer flow. Opening the gas-generator oxidizer control valve (GG OCV) increases total mass flow and raises the gas-generator (GG) gas temperature. Turbine power is increased and pump outlet pressures rises. Therefore, oxidizer and fuel flow rates increase for both for gas generator and thrust chamber.

By contrast, opening the GG fuel control valve mainly increases GG fuel flow while lowering the GG gas temperature, which reduces turbine power and thus pump outlet pressures and delivered flow rates. Consequently, the GG fuel valve is better suited for balancing the GG mixture ratio than for thrust throttling. As emphasized in the thesis, the GG temperature limit is critical due to turbine blade stress, because mixture ratio may deviate from on-design point, the GG fuel valve can be used to trimming mixture ratio to its design value and keep the turbine inlet temperature within limits.

The thrust-chamber fuel control valve (TC FCV) has only a modest system-level influence; it is more useful for trimming the chamber mixture ratio than for active thrust control. Throttling in this cycle is driven by gas-generator (GG) working gas. Opening the TC FCV reduces hydraulic resistance in the TC fuel line, so a larger share of pump-delivered fuel goes to the chamber and the GG fuel flow decreases. Thus, the TC FCV affects GG flow only indirectly and has a limited impact on overall system characteristics. Figure 5.31 shows that the thrust increases first, then decreases with the opening TC FCV. The increasing thrust is caused due to increasing flow rate first, but then temperature reduction be dominant at more fuel rich condition, therefore, thrust starts to decrease.

In summary, the control valve position effects on the system performance were studied and the developed model provides results how system characteristics changes with the changing hydraulic resistance using control valves.

7. FUTURE WORKS

The current thesis provides a comprehensive analysis of open-cycle LPRE modeling, and the obtained results are consistent with the literature. The developed model assumes prescribed temperatures at each engine station. Therefore, heat-transfer effects are not explicitly modeled. In future work, a heat transfer module can be developed to improve the accuracy of the predicted states and performance. In particular, regenerative cooling involves significant heat-transfer processes, but it is not currently included in the model. A thermal sub-model (e.g., regenerative cooling channels, hot-gas-side heat flux, and wall thermal inertia) can be formulated and integrated into the static model as a coupled submodule.

In addition, the static model can be extended to support systematic sensitivity analysis and uncertainty quantification to evaluate the effects of internal variations (e.g., manufacturing tolerances, design uncertainties) and external variations (e.g., ambient pressure and temperature). Thus, the engine performance dispersion can be found and the dominant parameters in crucial outputs such as chamber pressure, mixture ratio, turbopump speed, turbine power can be identified

Finally, future work may focus on control-oriented studies to maintain a constant mixture ratio while meeting thrust demand or on-design performance requirements. In this thesis, the impact of changing a single control valve position on engine characteristics was investigated. The positions of three control valves can be adjusted simultaneously to regulate flow rates and stabilize mixture ratio under disturbances. This approach can be evaluated using the dynamic model to compare control algorithms, valve actuator limits, and transient responses.

REFERENCES

[1] **Fernandez, L. A., Wiedemann C. and Braun V.** (2022). *Analysis of Space Launch Vehicle Failures and Post-Mission Disposal Statistics*, Aerotecnica Missili & Spazio, 101, 243-256

[2] **Sutton, G.P. and Biblarz, O.** (2016). *Rocket Propulsion Elements*, John Wiley & Sons, Nashville, TN, 9 edition.

[3] **Edberg, D. and Costa, W.** (2022). *Design of rockets and space launch vehicles,* American Institute of Aeronautics & Astronautics, Reston, VA, 2nd edition.

[4] **SpaceX** (2021). *Falcon User's Guide*

[5] **Praveen, R. S., Jayan, N., Bijukumar, K. S., Jayaprakash, J., Narayanan, V. and Ayyappan, G.** (2017). *Development of Cyrogenic Engine for GSLV MkIII: Technological Challenges,* IOP Conference Series: Materials Science and Engineering, Volume 171, doi:10.1088/1757-899X/171/1/012059

[6] **Almeida, D.S., Pagliuco, C.M.M.** (2014). *Development Status of L75: A Brazilian Liquid Propellant Rocket Engine,* J. Aerosp. Technol. Magan., Sao Jose dos Campos, Vol.6 No 4.

[7] **Lim, B., Kim, M., Kang D., Kim H. J., Kim, J. G. And Choi, H.S.** (2019). *Development of a Reliable Performance Gas Generator of 75 tonf-class Liquid Rocket Engine for the Korea Space Launch Vehicle II,* In Proceedings of the 8th European Conference for Aeronautics and Space Sciences (EUCASS), doi: 10.13009/EUCASS2019-521.

[8] **Kim, O., You, J., Park, S. and Jung, E.** (2016). *Components Layout Design of 75 tonf Liquid Rocket Engine,* In Proceedings of the 2016 KSPE Fall Conference, pp. 989-991.

[9] **Mason, J.R. and Southwick, R.D.Almeida, D.S.** (1989). *Large Liquid Rocket Engine Transient Simulation System.* NASA Technical Reports, National Aeronautics and Space Administration, pp. 167.

[10] **Binder, M., Tomsik, T. and Veres, J.P.** (1997). *RL10A-3-3A Rocket Engine Modeling Project,* NASA Technical Reports, National Aeronautics and Space Administration.

[11] **Majumdar, A.K., LeClair, A.C., Moore, R. and Schallhorn, P.A.** (2016). *Generalized Fluid System Simulation Program,* NASA Technical Publication, National Aeronautics and Space Administration, Marshall Space Flight Center and Kennedy Space Center.

[12] **EcosimPro ESPSS** (n.d.). *retrieved from https://www.ecosimpro.com/products/espss/* date retrieved 23.11.2025.

[13] **Park, S., Lee, E. and Lee, M.** (2024). *Monte-Carlo Simulation for Analyzing the Performance Variation of a Liquid Rocket Engine Using Gas-Generator Cycle,* Internatioal Journal of Aeronautical and Space Sciences, doi:10.1007/s42405-024-00760-2

[14] **Yamashiro, R., & Sippel, M.** (2012). Preliminary design study of staged combustion cycle rocket engine for spaceliner high-speed passenger transportatıon concept. *63rd International Astronautical Congress.* https://www.researchgate.net/publication/259896110.

[15] **Park, S.Y. and Cho, W.K.** (2018). *Program Development for the Mode Calculation of Gas Generator Liquid Rocket Engine,* Proceedings of 2008 KSPE Fall conference, pp. 366 – 370.

[16] **Cho, W.K. and Park, S.Y.** (2013). *Performance Sensitivity Analysis of Liquid Rocket Engine,* Aerospace Engineering and Technology, Vol. 12.

[17] **Cho, K.W. and Kim, C.** (2018). *Comparison of Effectiveness for Performance Tuning of Liquid Rocket Engine,* International Journal of Aerospace System Engineering, Vol. 5, No. 2, pp. 16 – 22**.**

[18] **Huzel, D. K., Huang, D. H.** (1967) Design of liquid propellant rocket engines. *NASA Space Vehicle Design Criteria*. SP-125. https://ntrs.nasa.gov/api/citations/19710019929

[19] **Gordon, S. & McBride, B. J.** (1994). Computer program for calculation of complex chemical equilibrium compositions and applications I. Analysis. NASA Reference Publication 1311. https://ntrs.nasa.gov/api/citations/19950013764

[20] **Hugh, B.M.** (1995). *Numerical Analysis of Existing Liquid Rocket Engines as a Design Process Starter,* AIAA, https://doi.org/10.2514/6.1995-2970.

[21] **Lim, B., Kim, M., Kang, D. and Choi, H.** (2020). *Development and Acceptance Test Results of 75-tonf Class Liquid Rocket Engine Gas Generator,* Journal of the Korean Society of Propulsion Engineers, Vol. 24, No. 4, pp. 55-65.

[22] **Haidn, O.J.** (2008). Advanced rocket engines. *In Advances on Propulsion Technology for High-Speed Aircraft* (pp. 6-1 – 6-40). Educational Notes RTO-EN-AVT-150, Paper 6. Neuilly-sur-Seine, France: RTO. http://www.rto.nato.int.

[23] **Kauffman, J., Herbetz, A., & Sippel, M.** (2001). Systems analysis of a high thrust, low-cost rocket engine. *4th International Conference on Green Propellants for Space Propulsion.* https://www.researchgate.net/publication/224789817

[24] **Lee, S., Lim, T. and Roh, T.S.** (2015). *Development of a System Analysis Program for a Liquid Rocket Engine*, Journal of Mechanical Science and Technology, doi: 10.1007/s12206-015-0535-x

[25] **Seo, S., Han, Y.M., Kim, S.K. and Choi, H.S.** (2006). *Study on Combustion Gas Properties of a Fuel Rich Gas Generator,* KSPE Spring Conference, pp. 118-122

[26] **Weiß, A.P.** (2015). *Volumetric expander versus turbine - which is the better choice for small ORC plants*, 3rd ASME ORC Conference, pp. 1–10.

[27] **Sobin, A.J. and Bissel, W.R**. (1974). *Turbopump Systems for Liquid Rocket Engines,* National Aeronautics and Space Administration

[28] **White, F. M.** (2003), *Fluid mechanics*, Fifth Edition, McGraw-Hill, New York, USA

[29] www.kari.re.kr

[30] **Choi, H.-S., Han, Y.-M., Kim, Y.-M., & Cho, K.-R.** (2009). *Development of a 30-ton-class LOX/kerosene rocket engine combustion device (I): Combustor*, Journal of the Korean Society for Aeronautical and Space Sciences*,* 37(10), 1027–1037

[31] **Choi, H.-S., Seo, S.-H., Kim, Y.-M., & Cho, K.-R.** (2009). *Development of a 30-ton-class LOX/kerosene rocket engine combustion device (II): Gas generator*, Journal of the Korean Society for Aeronautical and Space Sciences*, 37(10), 1038–1047*

[32] **Moon, Y., Park, S., and Jung, E.** (2016). *Startup Analysis of KSLV-II 75 tonf Class Liquid Rocket Engine*, 2016 KSPE Spring Conference, Korea, pp. 769-772.

[33] **Lim, B., Kim, M., Kang, D., Kim, H.-J., Kim, J.-G., and Choi, H.-S**. (2019). *Development of a Reliable Performance Gas Generator of 75 tonf-class Liquid Rocket Engine for the Korea Space Launch Vehicle II*, Proceedings of the 8th European Conference for Aeronautics and Space Sciences (EUCASS) doi: 10.13009/EUCASS2019-521.

[34] **Kim, S.K. et all.** (2010). *Analytical Considerations of Liquid Rocket Engine Thrust Chamber Design for the KSLV-II,* KSPE Journal, Vol. 4, pp. 71-80.

[35] **Choi, H.S. et all.** (2010). *Analysis of Pressure Fluctuations in 1/2.5-scale Thrust Chamber for 75tonf-class Engine*, KSPE Spring Conference, pp. 5-9

[36] **Han, Y.M. et all.** (2010). *Performance Prediction of Combustion Chamber for 75 ton LRE through Firing Tests at Low Pressure,* KSPE Spring Conference, pp. 66-70

[37] **Kim, J. et all.** (2010). *Low Pressure Combustion Tests for Technology Demonstration Model of 75 Tonf Thrust Chamber,* KSPE Spring Conference, pp. 10-13

[38] **Kim, J.S., Han, Y.M. and Ko, Y.** (2015). *Construction and Validation Test of Turbopump Real-propellant Test Facility,* Journal of the Korean Society of Propulsion Engineers, Vol. 19, No. 4, pp. 85-93

[39] **Jeong, E. et all** (2016). *Performance Test of a 75-tonf Rocket Engine Turbopump,* Journal of the Korean Society of Propulsion Engineers, Vol.20, No.2, pp. 86-93

[40] **Kim, D.J. et all** (2009). *Hydraulic Tests of Fuel Pump for 75-ton class Liquid Rocket Engines, KSPE Fall Conference, pp. 78-81*

[41] **Kim, D.J. et all** (2010). *Water Tests of LOX Pump for 75-ton Class Liquid Rocket Engine,* Aerospace Technology, Vol. 10, No.1

[42] **Lee, H., Shin, J., Jeong, E. and Choi, C.** (2016). *Turbine Performance Experiments for the Turbopump of a Liquid Rocket Engine,* International Journal of Aerospace System Engineering, Vol. 3, No. 1, pp. 25-29.

[43] **Jeon, J. et all** (2009). *A Study on the Force Balance of a Main Oxidizer shutoff Valve,* The Korean Society for Aeronautical & Space Sciences, Vol. 37, No. 8

[44] **Hong, M.** (2009). *Study on the Improvement in Cv of a Main Oxidizer Shut-off Valve,* Aerospace Engineering and Technology, Vol. 8, No.4.

[45] **Lee, J. and Lee, S.** (2012). *A study on the Characteristic of Fuel Shutoff Valve for 75 tonf Combustion Chamber,* Aerospace Engineering and Technology, Vol. 11, Issue 1, pp. 84-90.

[46] **Lee, J. and Huh, H.** (2010). *Dynamic Characteristics for Fuel Shutoff Valve of a Gas Generator,* Journal of the Korean Society of Propulsion Engineers, Vol. 14, Issue 4, pp. 1-9

[47] **Jang, G. W. et all.** (2010). *75-ton-class flow-control valve: Development report*. Hanwha Corp. [in Korean]

CURRICULUM VITAE

Name Surname **: Turan Çopuroğlu**

EDUCATION **:**

- **B.Sc.** **:** 2021, Istanbul Technical University, Faculty of Aeronautics and Astronautics, Astronautical Engineering
- **B.Sc.** **:** 2022, Istanbul Technical University, Faculty of Aeronautics and Astronautics, Aeronautical Engineering (Double Major)
- **M.Sc.** **:** 2026, Istanbul Technical University, Faculty of Aeronautics and Astronautics, Aeronautical and Astronautical Engineering

PROFESSIONAL EXPERIENCE AND REWARDS:

- 2021 - present Liquid Rocket Propulsion R&D Engineer, Roketsan

PUBLICATIONS, PRESENTATIONS AND PATENTS ON THE THESIS:

- **Çopuroğlu, T., & Edis F. O.** 2025: Liquid Propellant Rocket Engine Performance Sensitivity Analysis, IGRS, May 12-14, 2025 Istanbul, Turkey